Final Report

Characterizing Air Quality Impacts from Exceptional Events along the Wasatch Front

Prepared by:

Dr. Greg Carling
S-389 ESC
Brigham Young University
Provo, UT 84602
801-422-2622
greg.carling@byu.edu

and

Dr. Bradley Adams
360-I EB
Brigham Young University
Provo, UT 84602
801-422-6545
brad.adams@byu.edu

Project Period: July 1, 2019 – June 30, 2021

Report Submitted: November 24, 2021

Version 2 Submitted: May 23, 2022

Executive Summary

The overall goal of this study was to provide experimental and modeling data to better quantify the impacts of exceptional dust events on air quality and assess the impacts of future dust emission scenarios on PM concentrations in the Wasatch Front. Key results were as follows.

- Trace and major element concentrations were used to demonstrate differences between exceptional events and background sources. Measurements were made on existing PM_{10} filters from UDAQ during 2008–2009 and new PM samples collected at Provo during 2019–2020. Results showed winter periods during 2019 and 2020 had the highest concentrations of trace elements As, Cd, Fe, Mo, Pb, and Tl, with the highest concentrations in the $PM_{2.5}$ fraction, due to inputs of fine-particle urban pollution. Similar trends were found in the UDAQ PM_{10} filters collected at Salt Lake City during 2008-2009, suggesting these elements are commonly elevated during winter across the Wasatch Front. Periods of firework smoke in July had elevated concentrations of B, Co, Cr, Cu, K, and Sr. These elements were elevated in the Provo and Salt Lake City filters during July across multiple years and during January in some years. Filters collected during a dust event contained elevated concentrations of Ca, Li, Mg, Na, Sr, U, V, and Zn. The elements found in urban pollution, firework smoke, and dust events can be used to identify the impacts exceptional events across the Wasatch Front.
- Strontium isotope ($^{87}Sr/^{86}Sr$) ratios were used to identify PM sources to the Wasatch Front. Most Provo samples were within a narrow range of 0.709 to 0.710, which may be considered a background value for regional dust. Specifically, these values suggest inputs from Sevier Dry Lake dust throughout much of the study period. The elevated values during spring and fall of 2020 suggest dust inputs from Great Salt Lake. The lower values during July 2019, January 2020, and July 2020 are likely Sr-rich particles from firework smoke. Most SLC values ranged between 0.710 to 0.712, higher than values measured at Provo. The higher values likely reflect dust inputs from Great Salt Lake, a prominent dust source with a high $^{87}Sr/^{86}Sr$ ratio.
- A Utah-specific dust emission and transport model was developed based on WRF, CMAQ, and additional utility programs and property data. Comparison with AQS data for 2010 and 2017 dust events showed predicted peak $PM_{2.5}$ concentrations were ~35% lower (2010) and nearly 100% higher (2017), and timing of the peaks compared very well. Model sensitivity studies showed refinement in soil properties and dust flux parameters could improve model predictions. Dust origin and transport predictions from 2009 and 2020 were consistent with geologic markers ($^{87}Sr/^{86}Sr$ ratios) from filter measurements, including emissions from the Sevier Dry Lake and the GSL desert. The relatively brief nature of dust events can make comparison to filter data challenging. Results suggest the dust model is capable of accurately representing dust emission origins and transport direction during major dust events.
- Future impact scenarios were modeled to assess changes from a shrinking GSL and addition of multiple solar farms in Utah. For the April 2017 meteorological conditions, shrinking the GSL by 50-60% increased the peak dust concentration averaged across all AQS monitoring sites by 15%. The peak dust concentration in the local area surrounding the GSL shoreline was increased by 22 $\mu g/m^3$. The addition of multiple solar farms increased the peak dust concentration averaged across all monitoring stations by 14%. Dust concentrations in the areas immediately surrounding these theoretical solar farms increased but had lesser impact along the Wasatch Front. Different meteorological conditions could impact these values.

1. Background and Significance

Dust storms are exceptional events that negatively impact air quality across the Wasatch Front, yet it can be difficult to demonstrate the differences in particulate matter (PM) from urban versus regional dust sources, determine dust source locations contributing to these events, and predict future impacts under various land use and climate scenarios. Exceptional events are defined as unusual or naturally occurring events that can affect air quality but are not reasonably preventable or controllable using strategies implemented to attain federal air quality standards. These events, including dust and smoke from wildfires, are becoming more frequent in Utah, but their impact on ambient air quality and contribution to background levels are unclear and need further assessment. Demonstrating the occurrence of these events is important for regulatory purposes as Utah works to achieve air quality standards.

Dust storms occur frequently along the Wasatch Front with negative impacts on air quality (Hahnenberger and Nicoll, 2012; Steenburgh et al., 2012). The dry lakebed of Great Salt Lake (GSL) is a potent dust source located immediately adjacent to the Wasatch Front. As water levels continue to drop due to drought and diversions, dust storm events will likely increase in frequency and intensity in the future (Wurtsbaugh et al., 2017; Skiles et al., 2018). Proposed diversions on the Bear River would reduce water flow into the GSL further accelerate lake drawdown. Ultimately, decreasing water levels could create a "dust bowl" similar to Owens Dry Lake in California, where increased dust emissions have resulted in PM_{10} exceedances and deposition of harmful metals in downwind communities (Reheis, 1997; Reheis et al., 2002, 2009). Owens Lake bed was the largest single source of dust in the US, accounting for 5% of nationwide dust emissions, and is home to the highest atmospheric particulate and PM_{10} concentrations ever measured in the US that are 25 times higher than the federal limit (Gill and Gillette, 1991; Cahill et al., 1996). As lake levels decline, dust emissions from the GSL lakebed will likely increase and there will be an increased need to monitor for release of metals and other contaminants during wind events.

Tracking dust events between source locations and impacted areas is important for determining how future land use or water diversion schemes could alter dust source regions and affect downwind populated areas along the Wasatch Front. A better understanding of source-to-sink processes could inform future planning and resulting health impacts, especially for socioeconomically disadvantaged populations. Evaluating dust sources is nearly impossible with modelling or satellite imagery alone. Dust transport models that are supported by observational data are needed to apportion dust to specific emission sources. Transport models are useful for filling in gaps in spatial resolution from discrete point measurements, to provide a more complete understanding of source to receptor processes, and for predicting future impacts from various development schemes or water development projects. Combining observations and models is a powerful and novel method for exploring dust emissions, transport, and deposition.

Our study combines observational data in the form of chemical and isotopic measurements on air filter samples (Carling) to inform transport modeling (Adams) for dust source apportionment. We use specific dust events to evaluate dust sources using strontium isotope ($^{87}Sr/^{86}Sr$) fingerprinting to confirm the results of source tracking with the Community Multiscale Air Quality (CMAQ) transport model.

2. Purpose

The overall goal of our study is to provide experimental and modeling data to better quantify the impacts of exceptional dust events on air quality and assess the impacts of future dust emission scenarios on PM concentrations in the Wasatch Front. The study has four objectives:

1) Demonstrate differences between PM emissions from background sources and exceptional events using chemical signatures.
2) Identify dust source locations using isotopic "fingerprints".
3) Develop a dust modeling framework that is validated by published studies and isotopic data.
4) Use the validated dust model to predict impacts of future emissions under changing land use and climate conditions.

3. Methods and Results

3.1 Task 1 – Demonstrate Differences in PM Composition from Background Sources and Exceptional Events

3.1.1 Obtain existing PM_{10} filters from UDAQ

To quantify differences in chemistry between dust event days and other conditions, we obtained daily PM_{10} filters from UDAQ for trace element and isotopic analyses. The filters were from the Hawthorne monitoring station in Salt Lake City for the period 2008–2009, which were set for disposal and could be spared for chemical analyses. We analyzed a total of 30 filters for chemistry and $^{87}Sr/^{86}Sr$ ratios. The sample set includes filters from known dust event days and other conditions. We were unable to obtain more recent samples because they are potentially needed for regulatory purposes. For future studies, it would be worthwhile obtaining a larger sampling of PM_{10} filters for an analysis of PM chemistry across the Wasatch Front over time.

3.1.2 Collect new $PM_{2.5}$, PM_{10}, and TSP filters

To supplement the UDAQ PM_{10} filters, we collected biweekly PM samples at Provo from July 2019 through December 2020. The samples included $PM_{2.5}$, PM_{10} and total suspended particulate (TSP) filters using three MiniVol TAS Portable Air Samplers installed on the roof of the Eyring Science Center on the middle of BYU campus. Two-week periods were needed to obtain sufficient material on the filters for chemical and isotopic analyses. Over the 18-month period, we collected 39 $PM_{2.5}$ filters, 37 PM_{10} filters, and 39 TSP filters.

3.1.3 Laboratory analysis of PM filters

The $PM_{2.5}$, PM_{10}, and TSP filters were analyzed for trace element chemistry and $^{87}Sr/^{86}Sr$ ratios at the University of Utah. All 147 samples were analyzed for a suite of 40+ trace and major elements (including Ag, Al, As, Ba, Be, Ca, Cd, Co, Cr, Cu, Fe, K, Li, Mg, Mn, Mo, Na, Ni, P, Pb, REEs, S, Sb, Se, Sr, Ti, Tl, U, V, and Zn) using an Agilent ICP-MS. To prepare the filters for analysis, we use a two-step sequential extraction with 1 M acetic acid and aqua regia (a 1:3 mixture of concentrated nitric to hydrochloric acid). The signal from playa carbonate minerals (As, Ba, Ca, K, Li, Na, Sr, and U) is obtained from the first extraction step and the signal from urban combustion products or wildfires (Cd, Cr, Cu, Ni, Pb, REEs, Tl, V, Zn) is obtained from

the second extraction step. The primary goal for measuring trace element chemistry is to develop a library of chemical signatures of PM under various meteorological conditions (i.e., dust storms versus winter inversions or wildfire smoke). A secondary goal for measuring trace element chemistry is to determine potential health impacts of harmful trace metals adsorbed to the particles. The data collected in this project is useful for collecting an initial dataset of metal concentrations in PM across the Wasatch Front.

The PM filters were also analyzed for Sr isotope ratios to "fingerprint" dust from different source locations. The $^{87}Sr/^{86}Sr$ ratio is measured using a Neptune multicollector ICP-MS at the University of Utah. A minimum of 200 ng of Sr on the filter is required to make precise isotope ratio measurements. Six of the samples had insufficient Sr mass for the isotope measurement, giving a total of 141 $^{87}Sr/^{86}Sr$ measurements from filters on the acetic acid fraction. We used the acetic acid fraction for isotope measurements because it contains the calcite mineral fraction from playas and other dust sources.

3.1.4 Evaluate differences between urban pollution and exceptional events

Using the trace and major element measurements of $PM_{2.5}$, PM_{10}, and TSP samples collected under different air quality conditions, we can demonstrate the difference between ambient conditions and exceptional events. Figures 1, 2, and 3 show selected element concentrations collected for the three size fractions over the 18-month period of this study. The chemistry shows differences in element concentrations and element ratios during exceptional events and normal or background readings. Measured trace element concentrations showed distinct trends that reflect dust, winter inversions, and fireworks. Notably, we did not observe specific trends for wildfire events, possibly because wildfire smoke is primarily composed of organic material (ash) with low concentrations of inorganic metals. Elements that were correlated with windblown dust, with elevated concentrations in the PM_{10} fraction during a dusty period at the end of March 2020, included Ca, Li, Mg, Na, Sr, U, V, and Zn (Figure 1). These elements are typically contained in playa-type minerals common in northern Utah dust (Goodman et al., 2019). Another group of elements showed the highest concentrations in all size fractions during periods of winter inversions, including As, Cd, Fe, Mo, Pb, and Tl (Figure 2). These elements are associated with urban air pollution in northern Utah (Goodman et al., 2019). The highest concentrations were typically found in the $PM_{2.5}$ fraction, supporting the idea of fine-particle urban pollution. Similar trends were found in the UDAQ PM_{10} filters collected at Salt Lake City during 2008-2009, suggesting that these elements are commonly elevated during winter across the Wasatch Front over time. A third group of elements were elevated during July each year, reflecting inputs from firework pollution. The elements contributed by fireworks included B, Co, Cr, Cu, K, and Sr (Figure 3). Some of these elements were also elevated in January, another period of fireworks during New Year's celebrations. Many of the same elements were elevated in the Provo and Salt Lake City filters during July across multiple years.

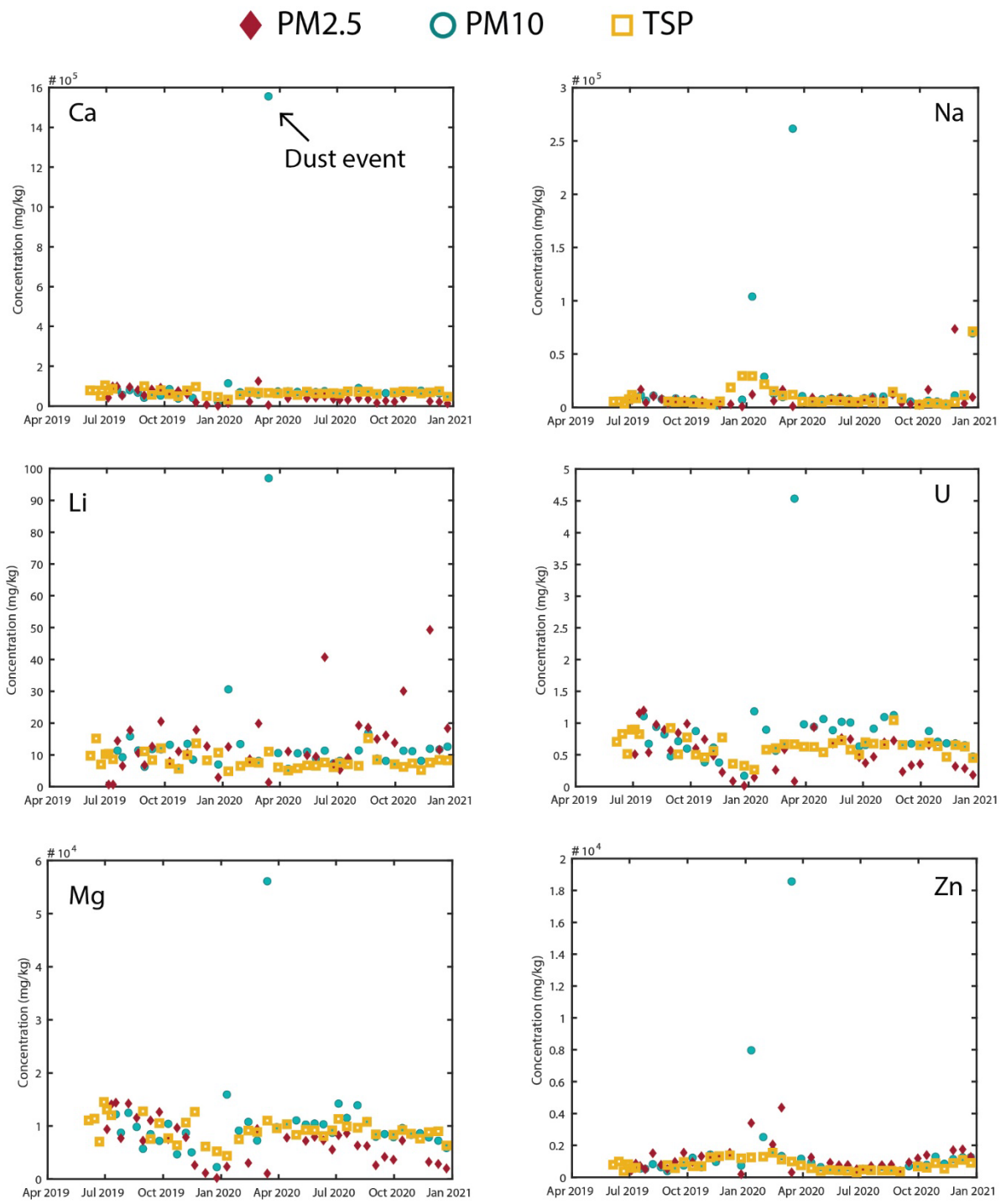

Figure 1. Elements with elevated concentrations in the PM_{10} fraction during a dusty period at the end of March 2020. These elements are typically associated with playa dust. Also, Sr showed a peak during the dust event (see Figure 3).

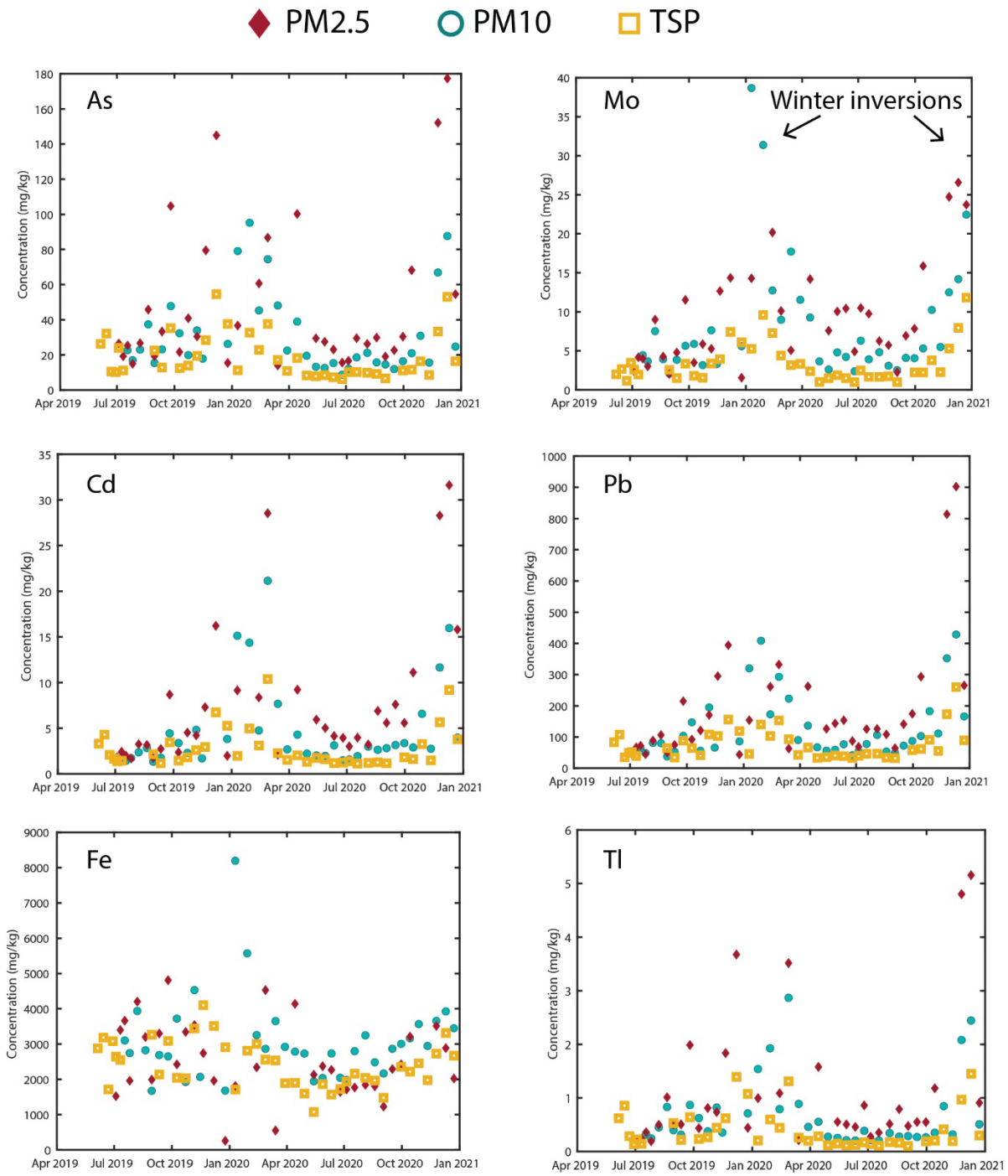

Figure 2. Elements with elevated concentrations during winter inversion periods. These elements are typically associated with urban pollution.

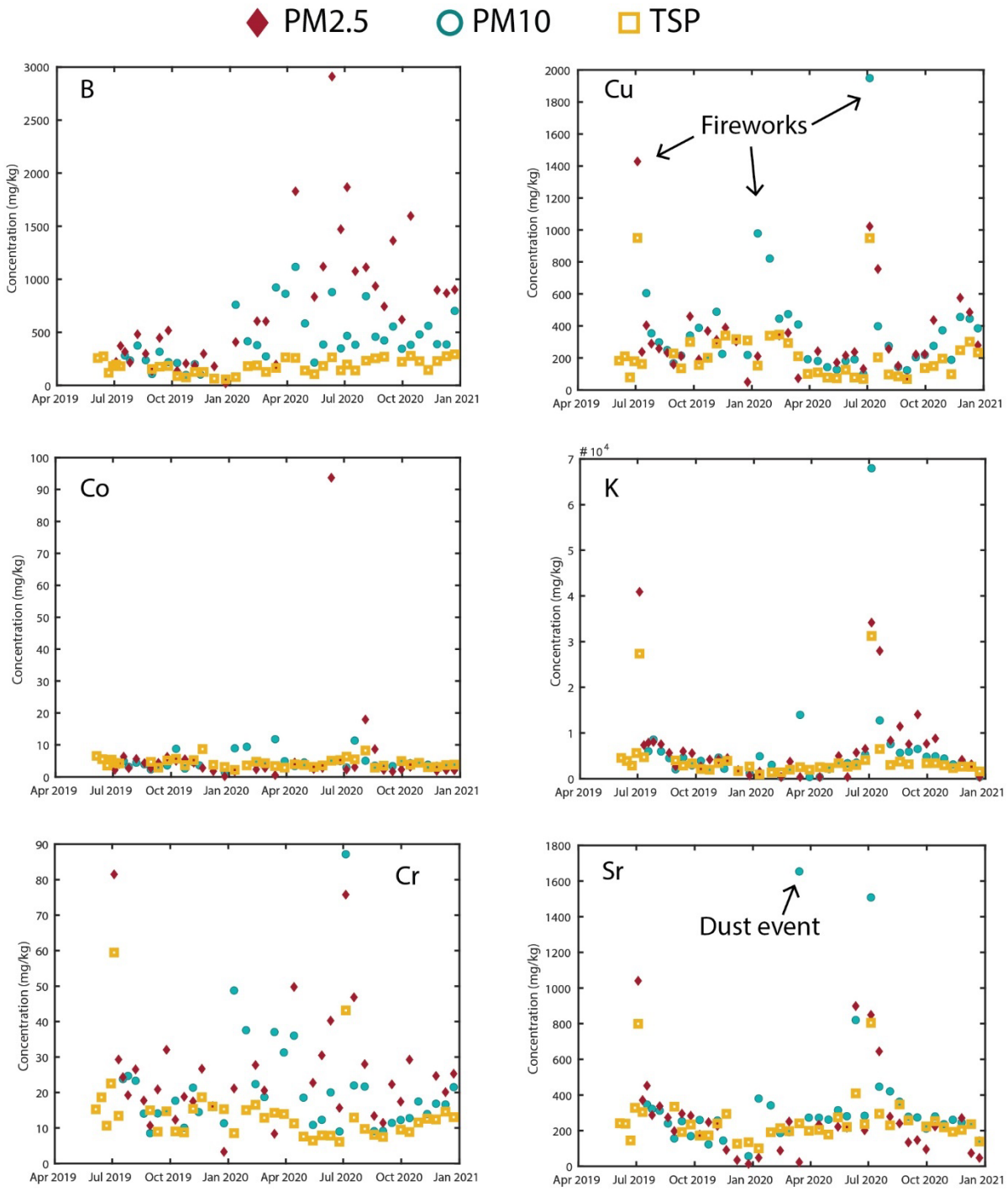

Figure 3. Elements with elevated concentrations during July (and January in some cases) due to pollution from firework smoke. Also, Sr showed a peak in March 2020 corresponding to a dust event.

We used Positive Matrix Factorization (PMF) and Principal Component Analysis (PCA) to investigate multivariate statistics on the PM filter chemistry. The EPA PMF 5.0 statistical model (https://www.epa.gov/air-research/epa-positive-matrix-factorization-50-fundamentals-and-user-guide) is a receptor model that is used to quantify contributions from various sources. PCA is an exploratory tool for investigating differences between the various sample types. Through the combination PMF and PCA statistical models, we can begin to develop a library of expected chemistry for "ambient" versus "exceptional events".

PMF was calculated from the concentrations of 41 elements measured on the acetic leach fraction on TSP filters. Elements excluded from the PMF were Ag, Cs and Th due to the high number of values below detection limit. Non-detect values in the remaining data were set at half the minimum concentration of each element to estimate low concentrations. Filters with <0.1 mg of dust were excluded from the PMF. The Base Model was run 20 times with a random seed to identify five factors. The Base Model Bootstrap Method was run using the auto-selected Base Model result.

The five factors are defined by distinct groups of elements that may reflect different sources (Table 1). Factor 1 is defined by high fractions of Li, Mg, Ca, and Sr, which are often associated with dust. However, Factor 1 also contains high fractions of rare earth elements and trace metals that are associated with other sources, so this factor is affected by additional inputs. Factor 2 is defined by more than 50% of As, Cd, Tl, and Pb and more than 20% of Cu, Sb, and Zn concentrations. These elements are associated industrial processes. Factor 3 contains 78.8% of La, which has been shown to be associated with oil refining (Goodman et al., 2019). Factor 4 is dominated by Na concentrations, which are associated with mineral dust from playas. Thus, dust may play a role in the signatures for factors 1 and 4. Factor 5 is explained by more than 30% of Ba, Cr, Cu, K and Sr concentrations. These elements are common components of fireworks.

Table 1. Percent abundance of elements in Factors 1-5 in the PMF statistical model.

	Factor 1	Factor 2	Factor 3	Factor 4	Factor 5
Li	47.4	7.2	29.7	10.0	5.6
Be	64.0	0.0	24.5	4.0	7.4
B	66.4	2.6	10.0	12.7	8.3
Na	0.0	0.0	21.9	78.1	0.0
Mg	59.0	2.1	23.4	5.9	9.6
Al	49.9	5.1	27.2	6.7	11.1
K	9.9	0.3	13.8	0.2	75.8
Ca	59.7	4.6	23.4	5.7	6.6
V	58.5	6.3	17.9	6.4	10.9

Cr	18.4	12.6	25.2	8.3	35.5
Mn	60.9	1.9	24.7	4.2	8.3
Fe	40.4	17.4	27.2	10.0	5.0
Co	55.7	4.4	24.9	6.3	8.8
Ni	52.4	10.0	24.0	9.4	4.2
Cu	0.0	27.8	18.5	8.8	44.8
Zn	30.4	28.0	24.1	15.2	2.3
Rb	49.3	7.2	20.6	6.9	16.0
Sr	46.4	0.0	16.8	4.7	32.1
Y	64.1	5.7	15.1	6.1	9.0
As	9.8	58.2	20.0	4.9	7.2
Mo	12.9	34.7	12.4	36.3	3.7
Se	26.2	13.7	46.9	7.2	5.9
Cd	13.2	69.5	4.4	7.1	5.8
Sb	22.2	25.4	30.9	17.4	4.1
Ba	20.0	17.1	14.3	10.9	37.7
La	21.1	0.0	78.8	0.0	0.1
Ce	72.1	7.8	0.0	8.9	11.2
Pr	60.0	5.1	20.2	5.9	8.9
Nd	59.2	5.5	19.4	6.6	9.2
Sm	60.5	3.9	20.1	7.0	8.5
Eu	57.4	6.2	19.6	7.7	9.2
Gd	61.3	4.2	19.6	6.0	8.8
Tb	63.7	4.3	17.2	6.7	8.1
Dy	62.7	5.3	17.1	6.2	8.6
Ho	64.2	3.6	17.6	6.0	8.6

Er	62.2	3.9	20.3	5.2	8.4
Yb	59.7	4.7	20.7	5.8	9.2
Lu	59.0	6.5	19.5	5.1	9.9
Tl	0.0	81.8	13.7	0.0	4.4
Pb	22.6	57.1	7.8	6.5	6.0
U	61.4	1.8	21.3	6.3	9.2

The PCA was created for the dataset in Matlab using concentrations measured in the acetic acid leachate for Provo filters and DAQ filters from Salt Lake City (Figure 4). The elements Ag, Cs and Th were excluded from the acetic acid PCA because of the high number of concentrations below detection limit. Concentrations of the remaining 41 elements below detection limit were set at half the minimum concentration of each element. Filters with <0.1 mg of dust were excluded from the PCA. Data were z-scored to normalize concentrations prior to running the PCA. In the PCA, principal component 1 (PC1) explained 36% of the variance in the dataset and PC2 explained 20%. PC 1 is positively affected by Al, As, B, Co, Fe, Li, Mg, Mn, Mo, Pb, Rb, Se, U, Y, Zn, and rare earth elements. PC 2 is positively affected by Be and Y, and negatively affected by As, B, Ba, Cd, Cu, Mo, Pb, Sb, Se, and Tl.

The PCA results show differences in the chemistry of $PM_{2.5}$, PM_{10}, and TSP filters at Provo. The TSP samples showed similar concentrations of most elements over time, making the samples cluster together in PCA space. In contrast, there was more variability in the chemistry of $PM_{2.5}$ and PM_{10} filters, making the samples more scattered across PCA space. The PM_{10} filters from the DAQ collector at Hawthorne plotted in a similar space as the Provo $PM_{2.5}$ and PM_{10} samples, giving confidence that the chemistry measurements are comparable between our samples and the DAQ samples. The groups of elements contributing to the PC scores may be useful for determining variability between background and exceptional events.

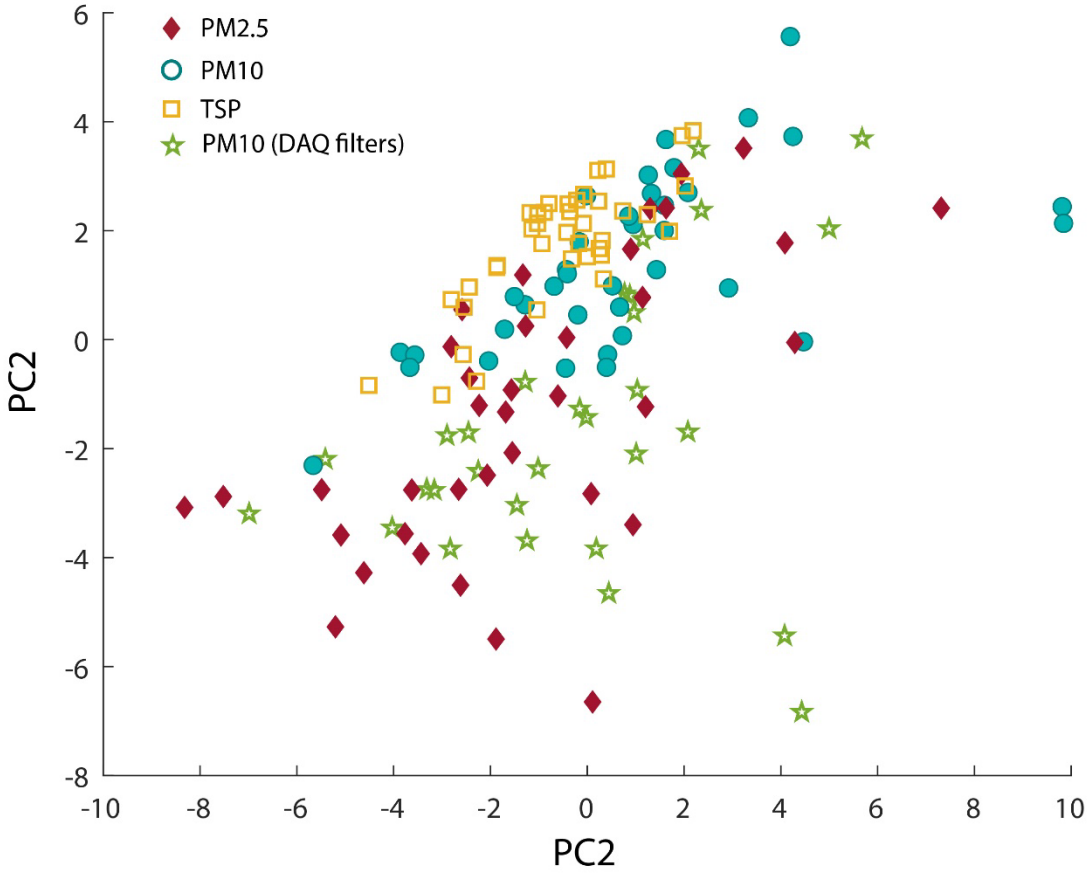

Figure 4. PCA for the acetic acid leachate data from Provo filters ($PM_{2.5}$, PM_{10}, TSP) and DAQ PM_{10} filters from Salt Lake City.

3.2 Task 2 – Identify Dust Source Locations Using Isotopic "Fingerprints"

Dust source locations are often not identifiable from modeling or satellite imagery alone, as these methods contain considerable uncertainties. Geochemical measurements provide an important constraint on modeling results. From previous research we developed isotopic "fingerprints" of major dust sources in western Utah including the Sevier Desert and Great Salt Lake (Carling et al., 2020). Sr isotope ($^{87}Sr/^{86}Sr$) ratios varied from 0.710 in the Sevier Desert to 0.715 at GSL (Figure 5), which is a wide range in values (relative to analytical errors on the order of ±0.00001) that provides leverage for discriminating the relative importance of dust from each source. Other playas, such as Tule Valley and the Bonneville Salt Flats, contained intermediate $^{87}Sr/^{86}Sr$ ratios of ~0.712 (Figure 5). Dust samples collected from Wasatch snowpack and the Wasatch Front had $^{87}Sr/^{86}Sr$ ratios falling within the range of the dust source locations (Figure 5), indicating that the playas are the major source of Sr to the Wasatch Front region. With the newly developed isotopic fingerprinting tool, we can begin to identify specific dust sources that affect the Wasatch Front and monitor changes over time. The source apportionment from isotopic measurements provides a constraint on modeling results. The feedback between geochemical observations and transport models will greatly improve dust apportionment studies and source tracking.

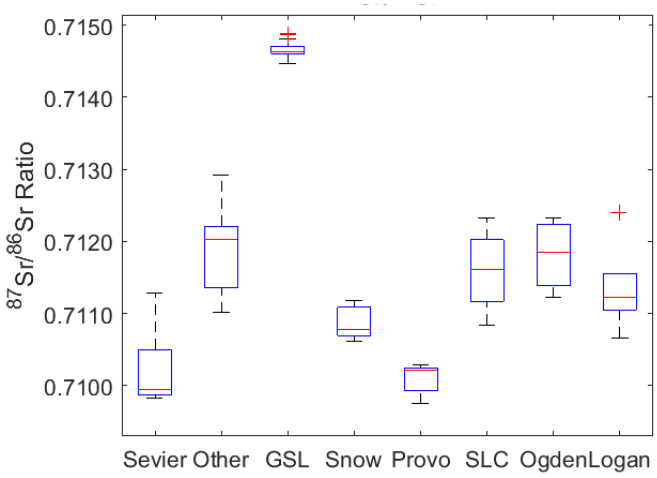

Figure 5. Sr isotope ($^{87}Sr/^{86}Sr$) ratios measured on dust samples from dust source locations in western Utah (Sevier Dry Lake, other playas, and Great Salt Lake) and dust samples collected from Wasatch snowpack and Wasatch Front urban area (Provo, Salt Lake City, Ogden, and Logan).

At our Provo site, the $^{87}Sr/^{86}Sr$ ratios varied throughout the study period from June 2019 through December 2020, with values ranging from 0.708 to 0.712 (Figure 6). For most time periods, the $^{87}Sr/^{86}Sr$ ratios were similar across size fractions suggesting minimal effects of size fractionation on the $^{87}Sr/^{86}Sr$ ratio. Most samples were within a narrow range of 0.709 to 0.710, which may be considered a background value for regional dust. Specifically, these values suggest inputs from Sevier Dry Lake (Figure 5) dust throughout much of the study period. The elevated values during spring and fall of 2020 suggest dust inputs from Great Salt Lake. The lower values during July 2019, January 2020, and July 2020 are likely Sr-rich particles from firework smoke.

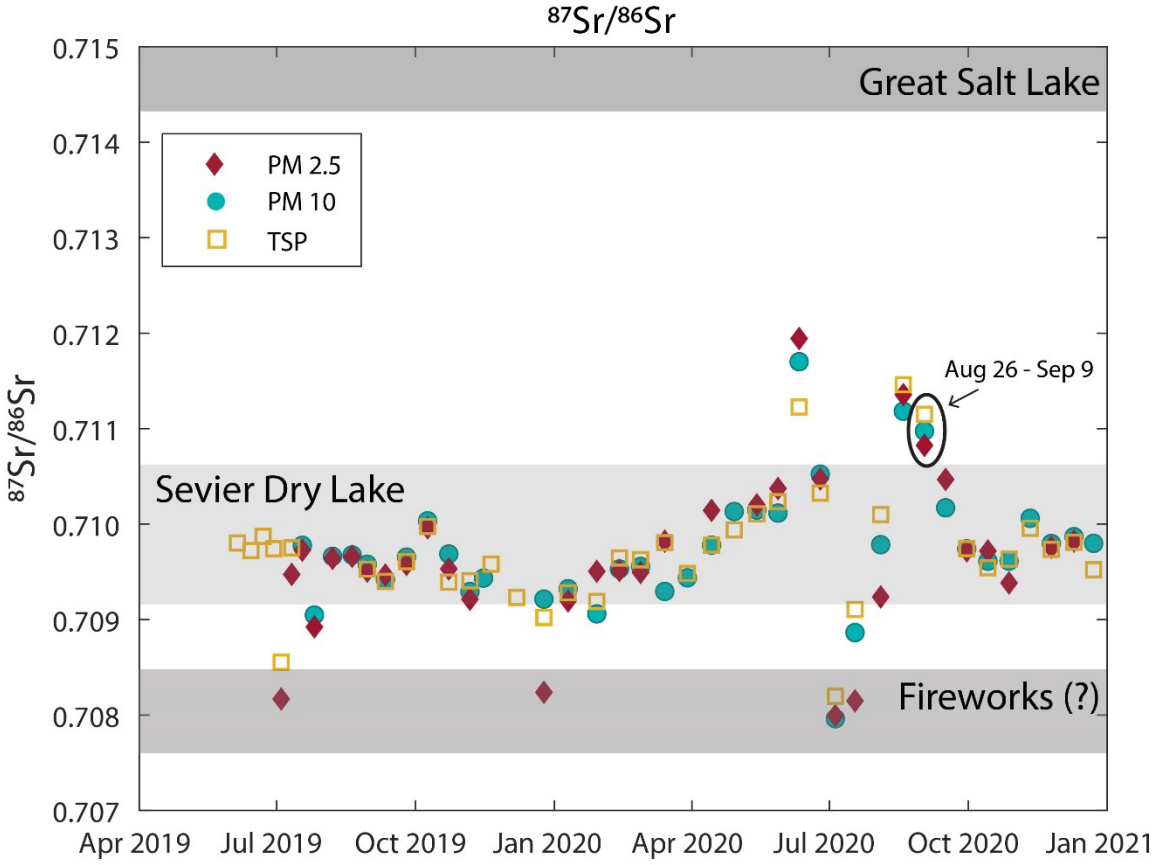

Figure 6. Sr isotope ($^{87}Sr/^{86}Sr$) ratios measured on $PM_{2.5}$, PM_{10}, and TSP filters at Provo, Utah, from June 2019 through December 2020. The $^{87}Sr/^{86}Sr$ ratios of potential sources are shown in horizontal bars to explain relatively low or high values throughout the sampling period. The dust event on September 8th, 2020, was captured in the filters (circled) collected over the period of August 26 – September 9, 2020.

Using archived PM_{10} filters from the Hawthorne station in Salt Lake City from August 2008 through September 2009, we measured $^{87}Sr/^{86}Sr$ ratios ranging from 0.709 to 0.715 (Figure 7). Most of the values ranged between 0.710 to 0.712, slightly higher than values measured at Provo (Figure 6). The higher values likely reflect dust inputs from Great Salt Lake, a prominent dust source with a high $^{87}Sr/^{86}Sr$ ratio (Figure 5). The lowest $^{87}Sr/^{86}Sr$ ratio was from July 2009, reflecting inputs of Sr from firework smoke. The lowest values from Provo and Salt Lake City were all measured during July, indicating an important Sr contribution from firework smoke across the Wasatch Front.

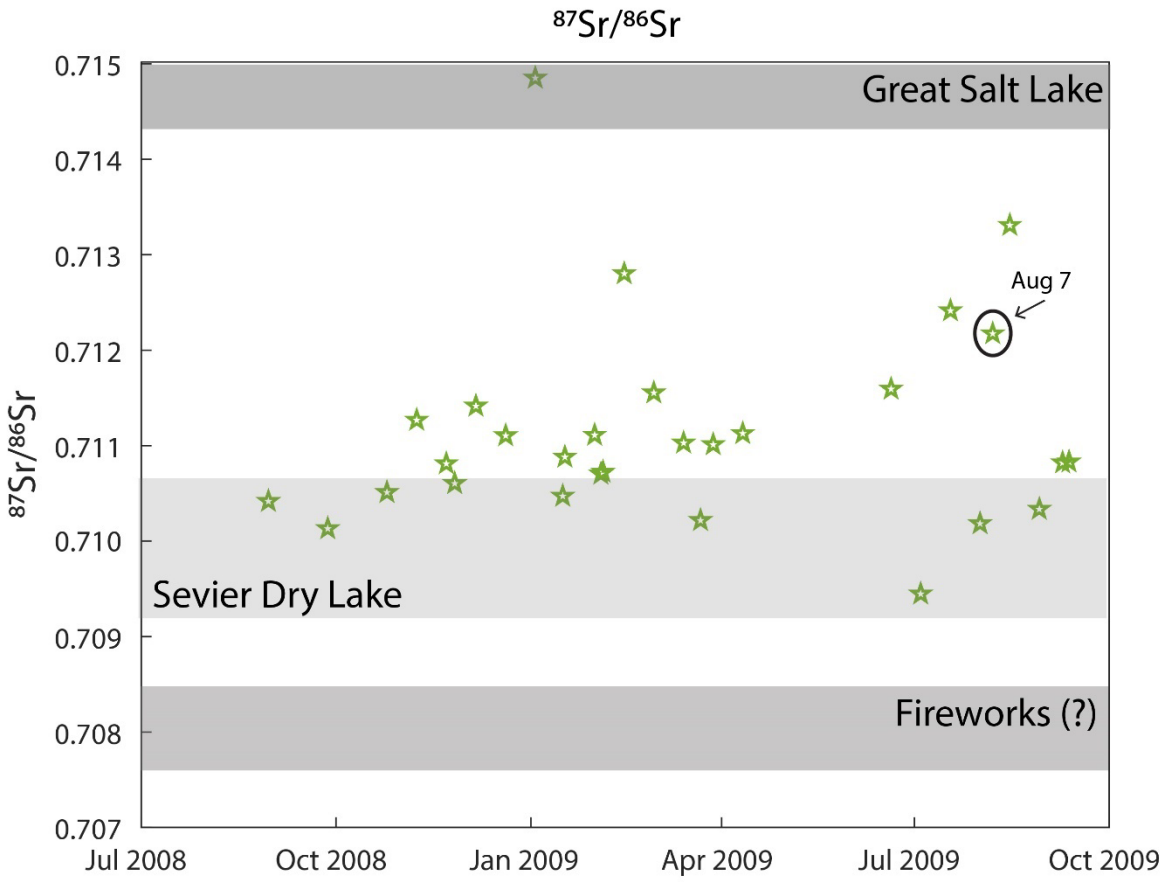

Figure 7. Sr isotope ($^{87}Sr/^{86}Sr$) ratios measured on PM_{10} at the Hawthorne UDAQ monitoring station in Salt Lake City from August 2008 through September 2009. The tail end of the dust event on August 7th, 2009, was captured in the filter identified with a circle.

3.3 Task 3 – Develop and Validate a Dust Emission and Transport Model

3.3.1 Develop dust emission and transport model framework

A dust emission and transport modeling framework has been developed based on the following key data sources and programs:

- National Center for Environmental Predictions, Final (NCEP FNL) Operational Analysis Data
- NCEP Automated Data Processing (ADP) Global Surface Observational Weather Data
- Weather Research and Forecasting (WRF) Model
- Community Multiscale Air Quality (CMAQ) Modeling System
- Atmospheric Model Evaluation Tool (AMET)
- Visual Environment for Rich Data Interpretation (VERDI) Tool

A visualization of this modeling framework is shown in Figure 8. There are several utility programs and property files that are used in conjunction with the main programs shown in Figure 8. Because there was limited documentation available for describing the overall modeling process used in this research, a User Guide was developed that lists the installation and operational process as well as required files for all programs used in the software framework (Lawless, et al., 2021). The User Guide is available at https://scholarsarchive.byu.edu/facpub/5515/.

Meteorological data is taken from the NCEP databases. This data consists of meteorological and land surface properties in 1-degree by 1-degree grids prepared operationally every 6 hours for the entire globe. Meteorological data is available on the surface, at 26 pressure levels, and the surface boundary layer. Relevant properties include surface pressure, sea level pressure, geopotential height, air temperature, sea surface temperature, soil moisture and temperature, relative humidity, horizontal u- (south to north) and v- (west to east) wind components, vertical motion, vorticity, and tropospheric ozone concentrations. All these parameters are necessary are for using the Pleim-Xiu Land Surface Model (PX-LSM) (Xiu and Pleim, 2001) in WRF which is required by the dust model in CMAQ.

WRF is a widely-used mesoscale weather prediction system that is used to process transient meteorological and land use data. The version used for this research is WRF v4.2.1. This model provides information for wind velocities, soil moisture, and snow cover which are used by the dust model in CMAQ.

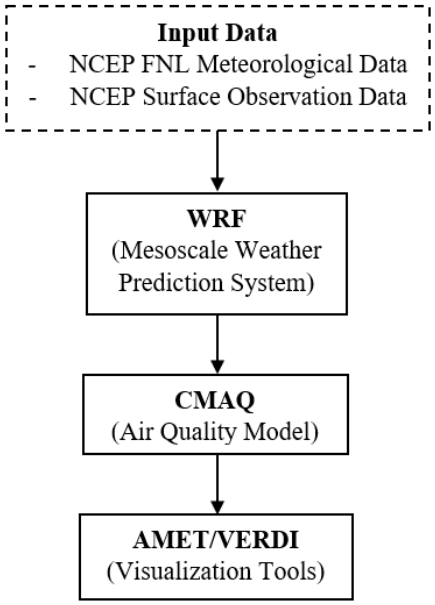

Figure 8. Visualization of the overall dust modeling framework. Input and output data required for each program are denoted with a dashed box. Note that utility programs associated with the major programs (in solid boxes) are not included here but will be shown later in the report.

CMAQ is the U.S. EPA default program for modeling transient air quality in the United States. CMAQ is an active open-source development project of the U.S. EPA that consists of a suite of programs for conducting air quality model simulations. CMAQ combines current knowledge in atmospheric science and air quality modeling, multi-processor computing techniques, and an open-source framework to deliver fast, technically sound estimates of ozone, particulates, toxics and acid deposition (USEPA, 2020b). For this research, CMAQ has been modified to focus only on dust predictions, thus reducing the need for extraneous air quality input data such as biogenic, automobile, and agricultural emissions which are not a focus of this study. Given that dust events have a short time span in which they occur turning off other background emissions should not impact the ability to model dust events. Focusing solely on dust emissions greatly reduces the preparation and computational time for CMAQ simulations.

Visualization and comparison to actual dust observations is accomplished by using the Atmospheric Model Evaluation Tool (AMET) and the Visual Environment for Rich Data Interpretation (VERDI) programs. AMET pairs observations and gridded model output in space and time to evaluate the model performance for a set of predicted or diagnosed atmospheric fields (Appel, 2019). AMET is used to evaluate the performance of the model by comparing dust predictions to actual observations. AMET ready observation data includes data from the Air Quality System (AQS) which will be used as the primary set of observations for comparison. AQS is an air pollution monitoring network that contains ambient air pollution data collected by EPA, state, local, and tribal air pollution control agencies (USEPA, 2020a). The Air Quality System (AQS) observations for $PM_{2.5}$ when available are used to compare against the predictions of the model. VERDI is a flexible, modular, Java-based program used for visualizing multivariate gridded meteorology, emissions and air quality modeling data created by

environmental modeling systems (USEPA, 2017). It is used to animate the predicted dust events and determine dust emission origins and transport paths.

Meteorological and Surface Observational Data

The Community Multiscale Air Quality (CMAQ) takes all its input data from Weather Research and Forecasting (WRF) outputs. WRF requires both static datasets and meteorological data as inputs. Static datasets are datasets that do not change from day to day such as surface elevation and land use (Wang et al., 2020). These datasets are discussed further in the following section. Meteorological data is taken from National Center for Environmental Predictions Final (NCEP FNL) Operational Analysis database (NCEP, 2000) as suggested by WRF. This data consists of 1-degree by 1-degree grids over the entire globe prepared operationally every 6 hours. Meteorological data is available on the surface, at 26 pressure levels, the surface boundary layer and at some sigma layers, the tropopause or the lowest layer of the atmosphere, and others. Sigma layers are based bases on scaled pressure levels commonly used in weather prediction models. Parameters include surface pressure, sea level pressure, geopotential height, temperature, sea surface temperature, soil values, ice cover, relative humidity, horizontal u- (south to north) and v- (west to east) wind components, vertical motion, vorticity, and ozone.

The observational data comes from NCEP Automated Data Processing (ADP) Global Surface Observational Weather Data (NCEP, 2004). According the NCAR research data archive, the NCEP ADP Global Surface Observational Weather Data are composed of surface weather reports operationally collected by NCEP. The data includes land and marine surface reports received via the Global Telecommunications System (GTS). Variables recorded in the reports include pressure, air temperature, dew point temperature, wind direction and speed. Precipitation data has been decoded for the U.S. and Canada. Report intervals range from hourly to every three hours. This data is used as it contained the important parameters of air temperature, surface winds, and snow cover.

The Weather Research and Forecasting Model

WRF is a mesoscale weather prediction system that was used to process the meteorological and land use data. The version used is WRF v4.2.1. This model provides information for wind velocities, soil moisture, and snow cover which are used by the dust model in CMAQ v5.3.1. As can be seen from Figure 9, meteorological data and static data are run through the WRF preprocessing system (WPS) where they are gridded onto the area of interest for the time period of interest. The output from WPS is then run through OBSGRID where surface observational data is incorporated. The output from OBSGRID is then sent to the WRF. The output from WRF is then sent to CMAQ.

As stated before, static datasets do not change from day to day and include data such as surface elevation and land use (Wang et al., 2020). High resolution versions are used for each of the mandatory datasets (WPS, 2021). These datasets have a resolution range of 0.9 to nine kilometers. It is worth noting that the static data, while relatively static, still contains transient elements. For example, the National Land Cover Database (NLCD) which provides land use data for WRF is static for the year in which it was created. Further, the NLCD is only updated once every five years and takes several years to verify and upload for public use. Because of this, the 2011 NLCD is used in this research. The Great Salt Lake (GSL) changes water levels throughout the year, and year to year, however it is modeled as static in the NLCD. This is a necessary

source of error that unfortunately is propagated in the model. WPS is responsible for mapping the meteorological and static data onto the simulation domain. Observational data is incorporated into the meteorological data using the WRF utility program OBSGRID. This updated meteorological data is then run through the WRF. Outputs from WRF and WPS are then used later in CMAQ.

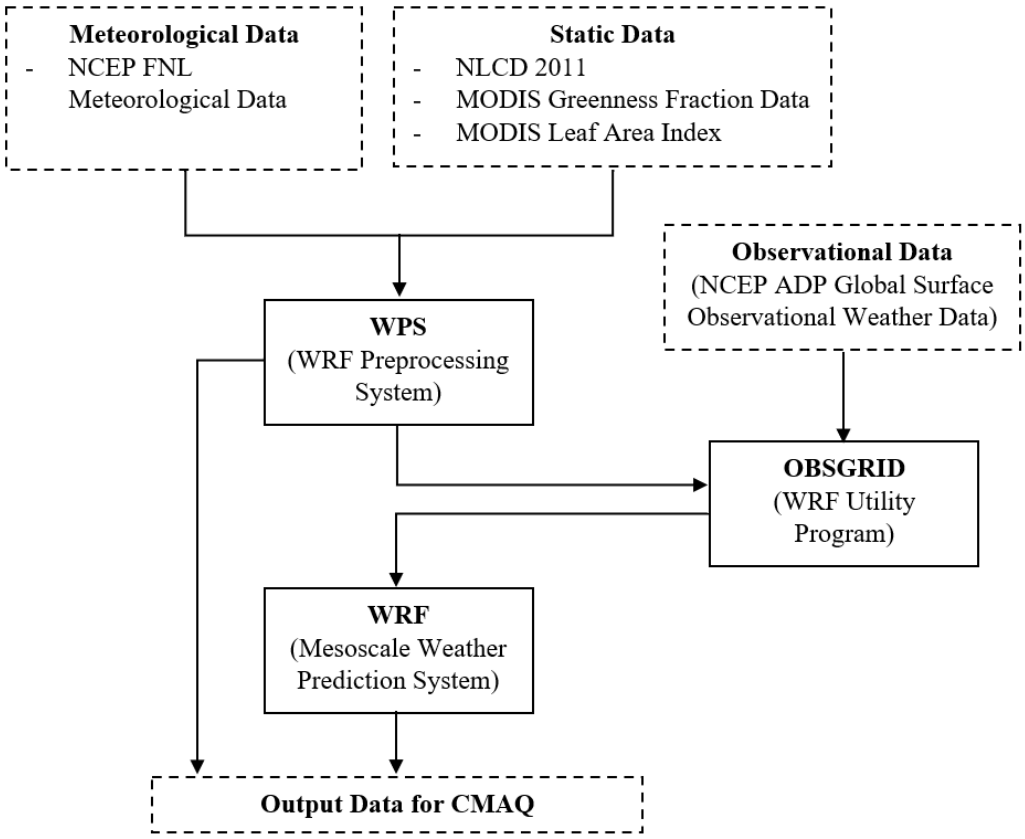

Figure 9. Overview of the WRF v4.2.1 modeling framework. Input and output data for each program are denoted with a dashed box.

Pleim-Xiu Land Surface Model

The Pleim-Xiu Land Surface Model (PX-LSM) is recommended when running the windblown dust emission model in CMAQ. As noted by Foroutan, the normally used Noah Land Surface Model calculates high levels of soil moisture content which completely suppresses dust emission (Foroutan et al., 2017). The PX-LSM is found to be more realistic and appropriate for the dust generation process in the CMAQ windblown dust module. This is due to its indirect nudging schemes. Nudging schemes use nudging coefficients in the model equations to relax the model state towards observations (Zou et al., 1992). There are two indirect nudging schemes included in the PX-LSM that correct biases in 2-m air temperature and relative humidity by dynamic adjustment of soil moisture and deep soil temperature (Gilliam and Pleim, 2015).

The recommended settings for using the PX-LSM in WRF and most of those used in this research can be found in the EPA online documentation "Overview of Science Processes in

CMAQ,", which includes subsections on “Description and Procedures for using the Pleim-Xiu LSM, ACM2 PBL and Pleim Surface Layer Scheme in WRF” (Gilliam and Pleim, 2015). These same settings were used for each dust event studied here, unless otherwise noted. The PX-LSM requires the use of the National Land Cover Database (NLCD) which supplies urban imperviousness, tree canopy, and land cover data. Accurate land cover data is essential for the CMAQ windblown dust model as only desert and crop land categories produce dust. The NLCD 2011 static data set provides a 9 second, ~250 m resolution for urban imperviousness, tree canopy, and land cover data. The NLCD 2011 data for Utah can be seen in Figure 10. Barren Land and Shrub/Scrub land use categories indicate where dust emission can possibly occur. The Great Salt Lake Desert can be seen to the west of the Great Salt Lake and is the biggest producer of dust in Utah. Additional emission sources occur farther south of this desert. Densely populated areas along the Wasatch Front can be seen in red to the east of the Great Salt Lake. It should be noted that although the NLCD 2016 has been released by the Multi-Resolution Land Characteristics Consortium (MRLC) it has not been formatted for use with WRF at the time of this writing.

According to Foroutan, “correctly representing the spatial and temporal variations in surface vegetation is important due to its various effects on dust generation including drag partitioning, local wind acceleration, near-source removal, and protective coverage” (Foroutan et al., 2017). The PX-LSM can also use more realistic time-varying vegetation fractions based on Moderate Resolution Imaging Spectroradiometer (MODIS) satellite data instead of the older weighting method that is based on lookup tables and land use fraction (Foley, 2020). This is done by incorporating the fraction of absorbed photosynthetically active radiation (FPAR), leaf area index (LAI), and albedo which are included in the MODIS static datasets (see Figure 9).

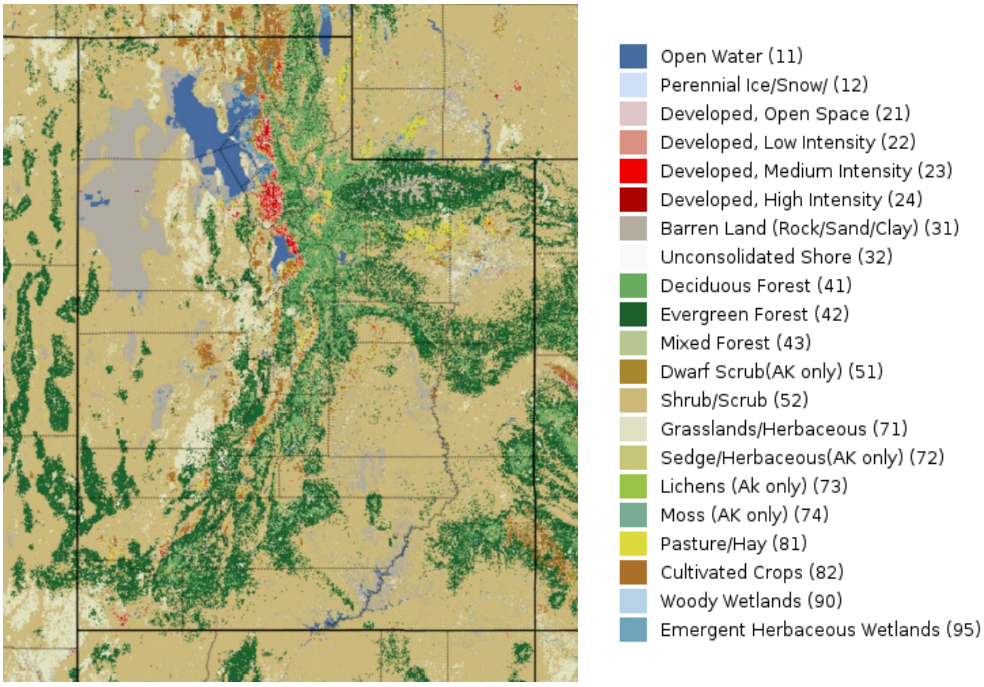

Figure 10. The 2011 National Land Cover Database (NLCD) map for the Utah region with land cover types.

As noted in the best practices guide, the PX-LSM snow cover model is quite simple and produces unrealistic results for snow cover that greatly affects dust emission. OBSGRID, a WRF utility program, can be used to incorporate snow cover and other surface observations that greatly increase the accuracy of the snow cover predictions.

OBSGRID

OBSGRID is an objective analysis tool offered as a utility program of WRF that, if used properly, can produce more accurate surface properties and thus help produce more realistic model results. The goal of objective analysis in meteorological modeling is to improve meteorological analyses (the first guess) on the mesoscale grid by incorporating information from observations (NCAR, 2021). While optional for other land surface models, the PX-LSM requires OBSGRID for its indirect soil nudging scheme and snow cover update. It does so by blending point surface observational data and forecast model initial conditions. A visualization of how OBSGRID is integrated into WRF can be seen in Figure 11. As stated previously, the output from the WRF Preprocessing System (WPS) is sent to OBSGRID where observational data is incorporated. The output from OBSGRID is then run through WRF.

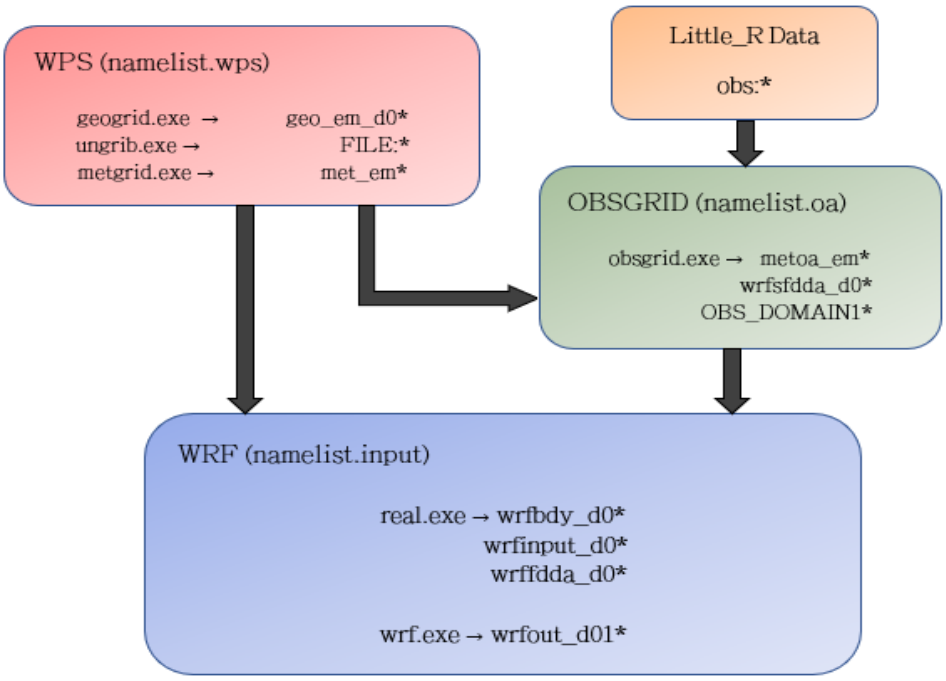

Figure 11. Detailed visualization of key steps and files for integrating OBSGRID into WRF.

OBSGRID, like several other WRF-related preprocessors, uses observational data in the LITTLE_R data format. The LITTLE_R file is an ASCII-based observation file format that acts as an intermediate file format between WRF and the many different observational data file formats (UCAR, 2021). Data formatted in LITTLE_R can be found at National Center for Atmospheric Research Data Archive (NCAR RDA). As mentioned previously, the data used for

this research comes from NCEP ADP Global Surface Observational Weather Data (NCEP, 2004). This data is specifically used to provide updated snow cover to the PX-LSM. Any form of snow cover results in the windblown dust model in CMAQ producing no dust. Using the baseline PX-LSM snow model for the April 2017 and March 2010 dust event cases results in little to no dust emissions due to incorrect snow cover. As can be seen in Figure 12, the use of OBSGRID to incorporate observational data greatly increases the accuracy of the snow cover WRF results.

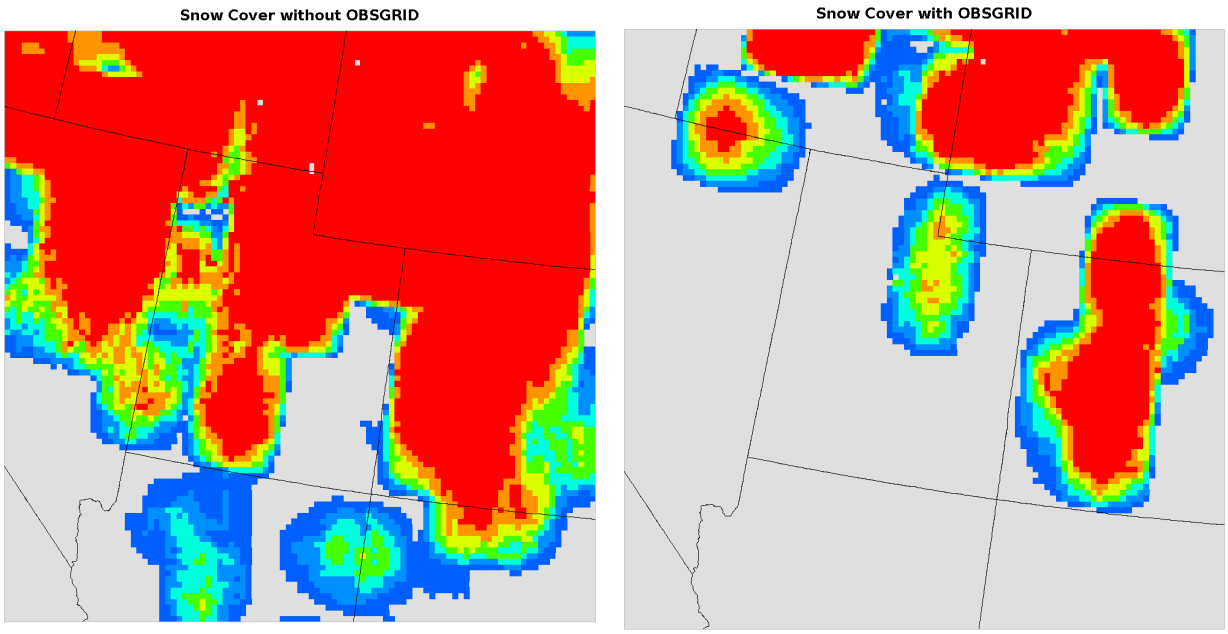

Figure 12. Snow cover for April 12, 2017 without (left) and with (right) OBSGRID. Note that colored areas do not emit dust in the CMAQ model.

In general, the use of the default settings is recommended when using OBSGRID. Table 2 includes the necessary inputs for the namelist.input that runs WRF to turn on the PX-LSM nudging. Table 3 details the specific variables in the namelist.oa used to run OBSGRID that are changed for both the 2017 and 2010 dust event cases and the reason for doing so. Appendix A contains the namelist.input and namelist.oa used for each case.

Table 2. Modifications to the Namelist.input for WRF to Enable PX-LSM Nudging.

Setting and Value	**Reason**
pxlsm_smois_init = 1	Necessary to initialize soil nudging in the PX-LSM.
pxlsm_soil_nudge = 1	Turns on soil nudging.
grid_fdda = 1	Turns on analysis nudging.

grid_sfdda = 1	Turns on 2D surface nudging and tells WRF to read in the wrfsfdda_d01 file from OBSGRID.

Table 3. Modifications to Namelist.oa for OBSGRID for 2010 and 2017 Dust Event Simulations.

Setting and Value	**Reason**
remove_data_above_qc_flag = 32768	Denotes a quality control flag that excludes data outside the analysis time. The different possible values for this QC flag can be found in the WRF User's Guide (Wang et al., 2018).
trim_domain = .TRUE	The domain is set up to include all of Utah and some of each neighboring state so the trim_domain keeps the focus of the analysis on Utah.
qc_test_buddy = .FALSE.	The buddy test, while highly recommended, works best with a great data density. We did not think our observations were dense enough for this setting to really be of benefit.
qc_test_vert_consistency = .TRUE.	This checks for spikes in the data and removes observations that do not realistically behave as its surrounding values. For a study as precise as dust emissions, this is very helpful.
qc_test_convective_adj = .TRUE.	This test confirms that none of the used values would contribute to an unstable rate and sorts the data accordingly.

Read_wrf_nc.exe

The overall goal of this project is to use the validated model framework to predict future dust events based on changes to existing dust emission sources or additions of new sources. To create or modify dust emission sources, WRF outputs are modified to introduce new land use, soil properties, soil moisture, and vegetation heights. This is done by using the read_wrf_nc.exe WRF post-processing utility (WRF, 2021). This post-processing utility uses user created subroutines to modify WRF output variables.

An example result from using one of the read_wrf_nc.exe subroutines created for this project can be seen in Figure 13. This subroutine decreased the water level and increased the shoreline around the Great Salt Lake (GSL) by 50 percent in an effort to represent the impact of drought or new water diversion policies. The left part of the figure shows the unmodified soil type around the GSL (shown in orange) whereas the right shows the increase in shoreline. Note that the soil type 2 (dark blue) does not depict a realistic soil type, but the color was used to highlight the soil type modification made with the subroutine.

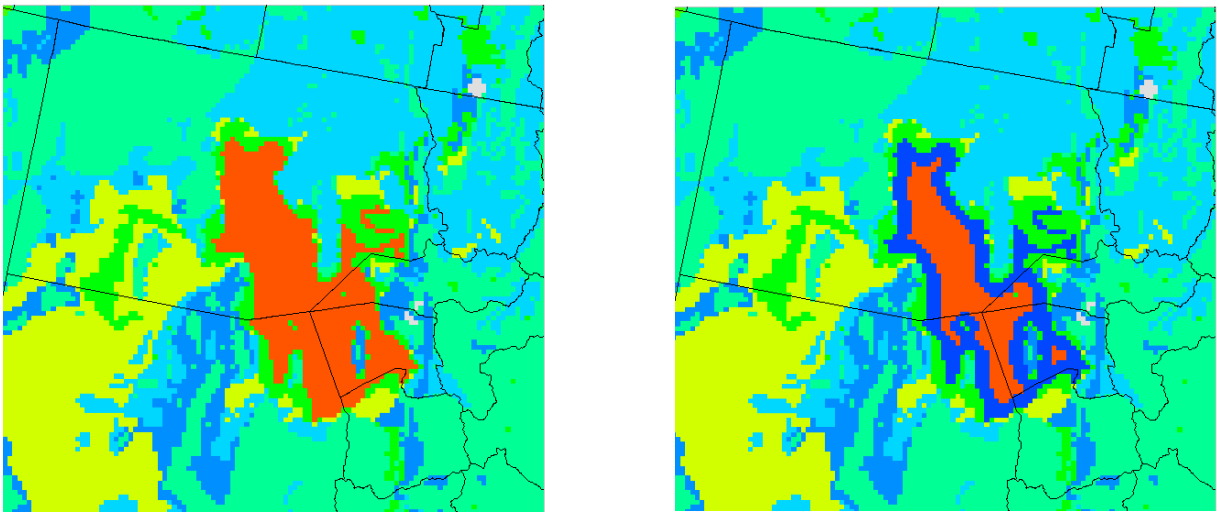

Figure 13. Baseline soil type around the Great Salt Lake (left, orange indicates water); soil type after subroutine used to increase the shoreline of the Great Salt Lake (right). The dark blue indicates the modified shoreline, i.e., conversion of water to barren land.

Community Multiscale Air Quality Modeling System

The Community Multiscale Air Quality Modeling System (CMAQ) was used to model windblown dust generation and transport. The version of CMAQ used in this project was CMAQ v5.3.1. CMAQ is a first-principles scientific computer model that comprehensively represents the most important processes affecting air quality and atmospheric chemistry (USEPA, 2021a). Figure 14 shows an overview of the CMAQ modeling framework. WRF outputs are processed through the Meteorology-Chemistry Interface Processor (MCIP) (USEPA, 2021b). MCIP processes the meteorological fields in the WRF output files into a format that is compatible with the CMAQ Chemistry Transport Model (CCTM). The output files generated by MCIP are used by Initial Conditions Processor (ICON) and Boundary Conditions Processor (BCON) to create the initial and boundary condition files respectively. The MCIP, ICON, and BCON output files are then input into CMAQ where they are used to predict dust emission and transport.

Normally CMAQ computes a variety of chemical reactions and species besides windblown dust concentrations. However, this requires a large amount of computational power and environmental data that have little to no impact on the windblown dust emission calculations. Modification of the CMAQ run script disables all calculations besides windblown dust. Note that this does not affect meteorological processes, such as rain or soil moisture change, which are computed WRF. This results in significant reductions in model setup time and calculation time. The modifications can be seen in Table 4 below. All other settings are left at the default values. Modification of the windblown dust module is accomplished by changing parameters in the DUST_EMIS.F file.

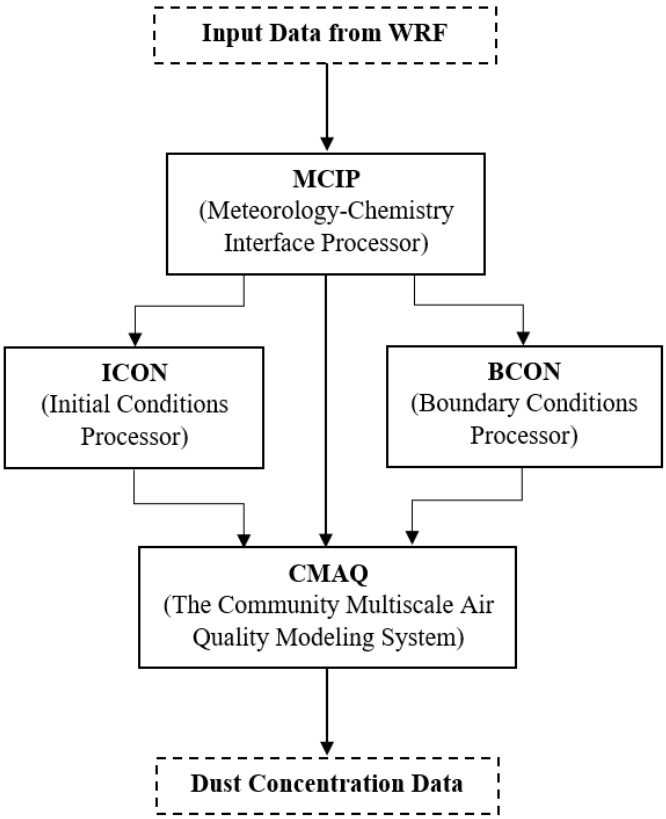

Figure 14. Overview of the CMAQ v5.3.1 modeling framework. Input and output data required for each program are denoted with a dashed box.

Table 4. CMAQ Run Script Settings Used to Turn Off Everything Except Windblown Dust Calculations.

Setting and Value	Reason
Science Options	
CTM_OCEAN_CHEM N	Focus is on Utah so no need for ocean halogen chemistry and sea spray aerosol emissions
CTM_WB_DUST = Y	Uses the inline windblown dust emissions
CTM_WBDUST_BELD = UNKOWN	Use land use information provided by MCIP for windblown dust calculations
PX_VERSION = Y	Indicates that the Pleim-Xiu land-surface model was used. The Pleim-Xiu model is necessary for the windblown dust module in CMAQ
CLM_VERSION = N	Only one land-surface model can be used
NOAH_VERSION = N	Only one land-surface model can be used
CTM_BIDI_FERT_NH3 = F	No emissions besides windblown dust and therefore not necessary
CTM_SFC_HONO = N	No emissions besides windblown dust and therefore not necessary
I/O Controls	
CTM_EMISCHK = N	Since no emissions sources are provided this stops CMAQ from aborting when it finds no Emissions Input files.

Verification (AMET) and Visualization (VERDI) Tools

Visualization and comparison to actual dust observations is accomplished by using the Atmospheric Model Evaluation Tool (AMET) and the Visual Environment for Rich Data Interpretation (VERDI) programs. AMET pairs observations and gridded model output in space and time to evaluate the model performance (Appel, 2019). AMET is used to evaluate model performance by comparing predicted dust concentrations to observed or measured concentrations from either sensor networks or specific monitoring stations. An example of this can be seen in Figure 15 which shows predicted $PM_{2.5}$ concentrations compared to observed $PM_{2.5}$ concentrations from the Air Quality System (AQS) sensor network.

There are numerous AQS observation sites for $PM_{2.5}$ across the state of Utah, thus it is convenient to use these measurements to compare against model predictions. The US AQS sensor network contains ambient air pollution data collected by EPA, state, local, and tribal air pollution control agencies from over thousands of monitors (USEPA, 2020a). The AQS has

extensive history of being used to assess air quality, perform modeling for permit review analysis, and prepare reports for Congress as mandated by the Clean Air Act. The locations of the AQS stations in Utah used for this research can be seen in Figure 16 for 2010 (left) and 2017 (right). Note the increase in observation sites along the Wasatch Front region over time. This means comparisons done in 2017 are more heavily weighted to this region.

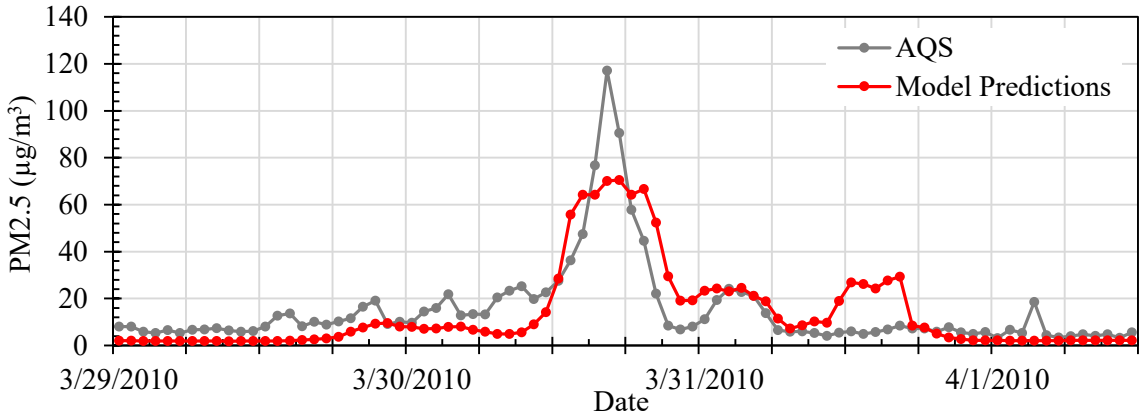

Figure 15. Example of modeled $PM_{2.5}$ compared to observed concentrations recorded by the Air Quality System (AQS) sensor network.

The dust model predicts $PM_{2.5}$ concentrations at multiple elevation levels and then averages across all elevation levels to produce one $PM_{2.5}$ concentration for each grid cell. Observations of $PM_{2.5}$ concentrations are taken by each monitoring station. These observations are averaged to produce hourly concentrations that are then compared to the model predicted concentrations. The modeled concentration in the grid cell corresponding to the location of the observation site is compared that observation sites observed concentrations. If there are multiple stations in one grid cell, each of their observations are averaged to produce one observed concentration value for that grid cell. When doing a comparison of the whole grid, each observation site's observed concentration and the corresponding grid cell are averaged together and compared. Further explanation of how comparison in AMET works can be found in Atmospheric Model Evaluation Tool v1.4 User's Guide (Appel, 2019).

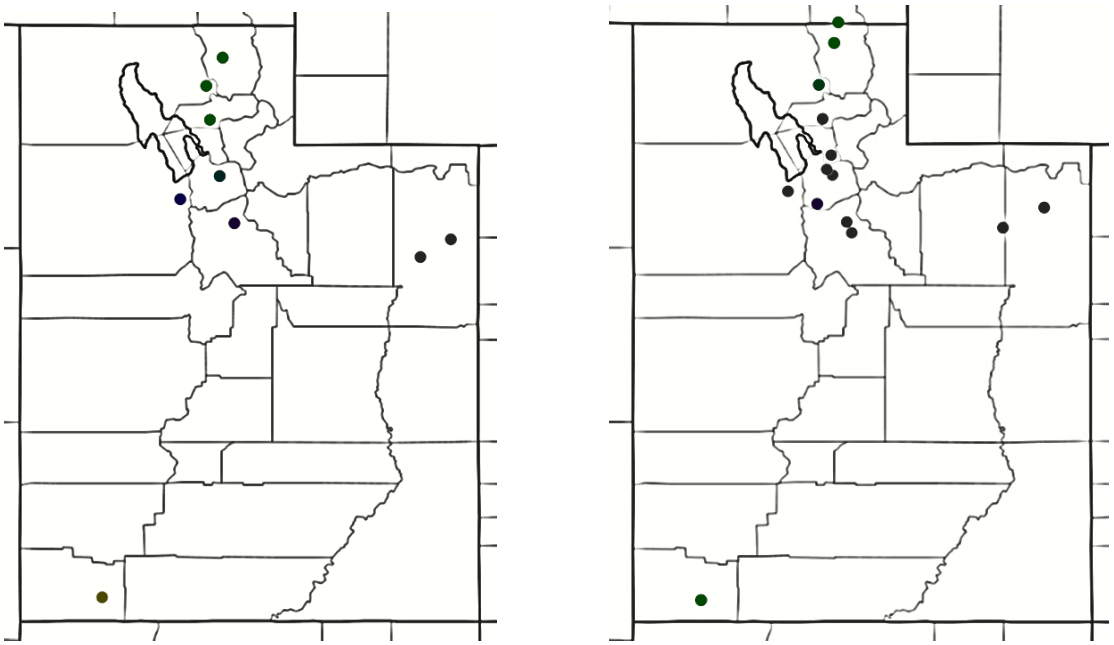

Figure 16. Location comparison of Air Quality System monitoring stations for 2010 (left) and 2017 (right).

It should be noted that dust typically contains particles greater than 2.5 μm. PM_{10} measurements (which include particles up to 10 μm) will contain more particles that are representative of dust particle size distribution, however nearly all sensor networks focus on $PM_{2.5}$ measurements because they are of greater interest to the health science community. These measurements accurately represent the occurrence of dust events, if not the precise concentrations of all dust particle sizes. This discrepancy contributes to the uncertainty of AQS measured dust concentrations. Observational data from sites used in previous studies in literature are input into AMET and used to validate the model.

VERDI is a flexible, modular, Java-based program used for visualizing multivariate gridded meteorology, emissions and air quality data created by environmental modeling systems (USEPA, 2017). It is used to animate predicted dust events and determine their origin and produce static plots of dust concentrations and other properties. For example, VERDI helps with performing future impact studies by visualizing the soil types and land use that changed.

3.3.2 Model Verification from Literature

Two dust events previously studied and published were used to verify model results and to guide adjustment of correction parameters to fit Utah soil properties. The first published event is from an April 2017 dust event (Skiles, et al., 2018) and the second is from a March 2010 dust event (Mallia, et al., 2017). Data from air monitoring stations for each dust event were used to compare the model predictions to actual observations. Despite the assumption that the model needs correction parameters to fit Utah soils, the baseline model framework performed was able to predict dust events within the targeted event timing and relative magnitude of 1-3 times observed

concentrations. This will be shown in subsequent sections. Based on this, it was determined that no significant corrections to the dust emission model parameters were required.

However, modeling these events indicated that predicted results were sensitive to soil properties and land use types (as opposed to model parameters). This suggests that further experimental data is required to confirm or improve the soil properties assumed in the dust emission model. Sensitivity studies are performed on three of these properties; soil composition, flux factors, and salt correction factors. These sensitivity studies can show which experimental data should be prioritized in future research to improve the dust emissions model when modeling Utah specific dust storms. These sensitivity studies are further discussed after the verification studies.

Historically, dust modeling has had a high level of uncertainty. As noted by Foroutan, multiple studies show large diversity between models (Foroutan, et al., 2017). Dust emission models can show differences in predicted dust concentrations up to four times different with some showing order of magnitude differences (Todd, et al., 2008; Uno, et al., 2006). This high level of uncertainty can be attributed to the fact that dust emission involves several complex and nonlinear processes governed by meteorology, land surface, and soil texture (Foroutan, et al., 2017). Similarly, dust measurements are difficult due to the variable size of the dust particles (e.g., dust particles can range from 0.3 to 1000 μm and dust from the silty loam playas in Utah are generally in the 0.5 to 100 μm range (Li, et al, 2018) whereas $PM_{2.5}$ sensors can measure only up to 2.5 μm particles), the orientation of the sensors with respect to the wind direction, the dynamic nature of the dust events (e.g., difficult to track deposited dust mass as a function of time), and differentiating dust $PM_{2.5}$ from other $PM_{2.5}$ particulates. As stated previously in Section 1.2, given the uncertainty of the model inputs, combined with uncertainties in the dust measurements, model results that predict the dust concentrations within a factor of 1-3 times the magnitude of the observations are considered accurate for modeling dust events in Utah.

April 2017 Event

The April 2017 dust event comes from the paper "Implications of a shrinking Great Salt Lake for dust on snow deposition in the Wasatch Mountains, UT, as informed by a source to sink case study from the 13–14 April 2017 dust event" by Skiles et al. (2018). This event was the result of a cold front moving in from the Pacific Northwest and strong winds coming from the southwestern Utah. This event lasted from late April 13th into early the next day. A snapshot of the winds at the peak of the dust event is shown in Figure 17. This plot shows atmospheric wind velocities at an elevation of 600 mbar (0.6 atm) which give an overview of where dust is transported once saltation occurs; this is not the 10-m wind velocities which would correlate with dust emission sources. Figure 17 uses standard wind barb notation. The tip of the shaft denotes the location of the wind speed and direction being shown. Wind speed is denoted by the number of barbs on the feather where each full barb represents a speed of 10 knots with a pennant representing 50 knots. Wind speed is also given in meters per second. Wind direction is given by following the shaft from feather to tip. The strong winds coming from the cold front increase dust emission over the GSLD and the southwestern winds flowing to northeastern Utah will carry dust from emission sources in southwestern Utah. These same southwesterly winds will carry dust over the Great Salt Lake rather than over more densely populated regions along the Wasatch Front. If the winds were more directly from the west, dust emissions from the GSLD would be expected to be carried more directly over populated regions directly east of the GSLD such as Salt Lake City.

Results spanning the dust event can be seen in Figure 18, which shows predicted $PM_{2.5}$ concentrations compared to actual observations from the Air Quality System (AQS) network for all of Utah. Note that while the entire computational grid includes areas of surrounding states, only monitoring stations located in Utah were used for the observations and comparisons (i.e., only model results co-located with Utah observation sites were used in the comparison). As can be seen from the figure, the model is able to adequately capture the timing but overpredicts the peak magnitude of the dust event by a factor of 2-3. Peak $PM_{2.5}$ concentrations differ by 247 percent. It should be noted that the days preceding the event have similar dust concentration magnitudes to the dust event on the 13th. These concentrations can be attributed to non-dust background $PM_{2.5}$ particulates caused by industry and transportation air pollutants. The days after the dust event show this background $PM_{2.5}$ was reduced by the storm winds (i.e., the air was cleared as the storm front moves through the area). The model is also able to predict this drop off.

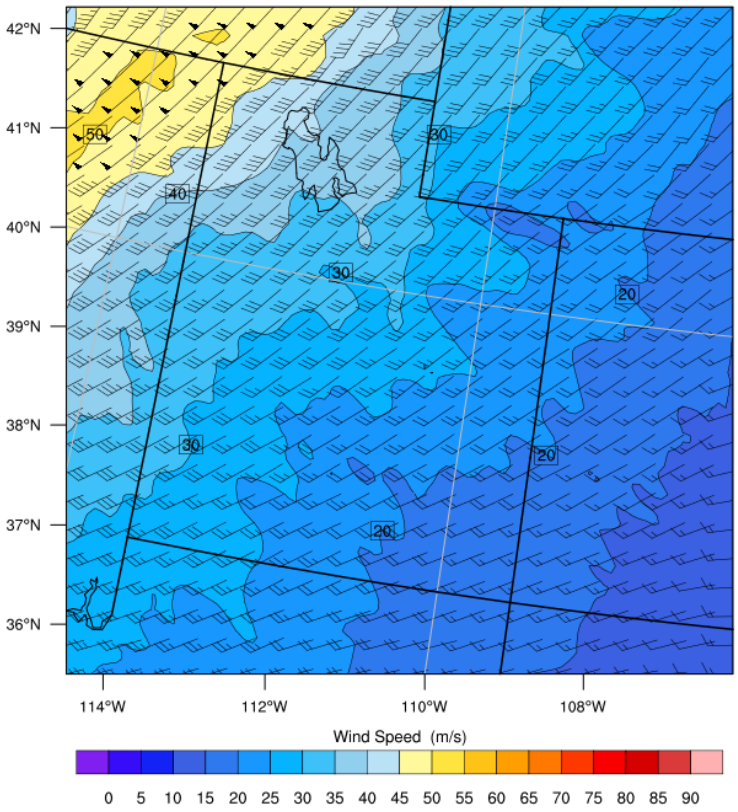

Figure 17. Snapshot of wind conditions during the April 2017 Dust event. Note the strong cold front outlined in yellow coming from the Northwest. Wind velocities are at 600 mbar. Wind barbs use standard wind barb notation. Wind speed is denoted by the number of barbs on the feather where each full barb represents a speed of 10 knots with a pennant representing 50 knots. Wind speed is also given in meters per second (0-90 m/s scale). Wind direction is given by following the shaft from feather to tip.

The difference between the predicted and observed magnitudes can be attributed to uncertainties in measurements and in the meteorological fields and land use properties produced by WRF that are then fed into CMAQ. As noted by Foroutan, high level of uncertainty in modeling dust

emission can be attributed to the fact that dust emission involves several complex and nonlinear processes that are governed by the meteorology, land surface, and soil texture (Foroutan, et al., 2017). Small uncertainties in modeling these inputs and properties can propagate throughout the model to create large uncertainty in modeled dust emissions.

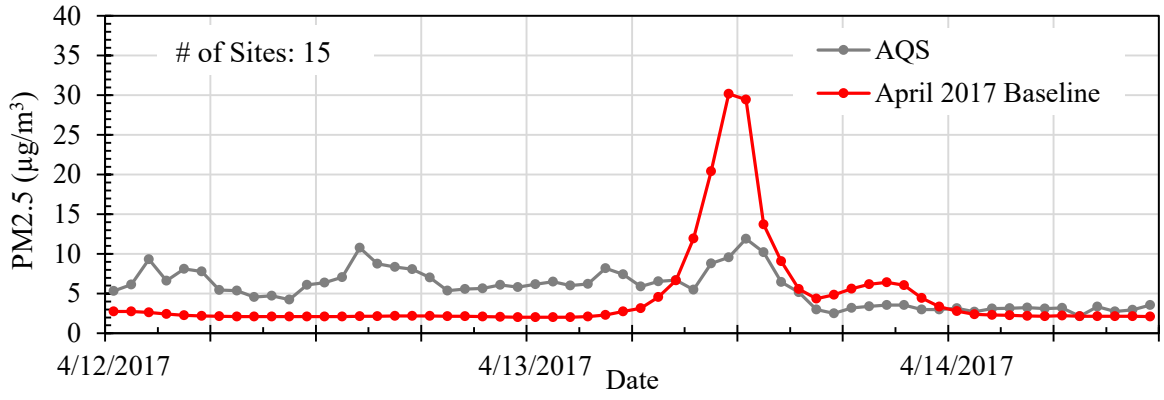

Figure 18. Baseline model results compared to observational data for the April 13-14, 2017 dust event for all of Utah. Note that the number of sites used for the observations during this time period is given in the upper left corner.

In the paper by Skiles et al., the Atwater Study Plot (ASP) provides an additional $PM_{2.5}$ observation site. The ASP is located in Little Cottonwood Canyon, UT (40.591206° N, 111.637685° W) which can be seen in Figure 19. CMAQ predictions are compared to the ASP observations as shown in Figure 20. As can be seen CMAQ underpredicts the magnitude of the dust storm observed at the ASP by 68 percent, however the timing lines up with the dust event. While the differences in magnitude fall within the defined (1-3X) tolerance for accuracy, some specific characteristics of this measurement site and time can provide further insight into potential reasons for the discrepancies. The ASP is located deep in a canyon where meteorological fields are difficult to accurately model. The topography varies greatly over just 1 km. As mentioned previously, the lowest resolution possible in static datasets given by WRF is 0.9 km which would not accurately model this topography. Accurately resolving this geography with the 8 km grid used for this research is virtually impossible. The 8 km resolution was chosen because obtaining grid resolution on a 1 km scale increases the computational cost to a point that it is not feasible to model the full Utah region.

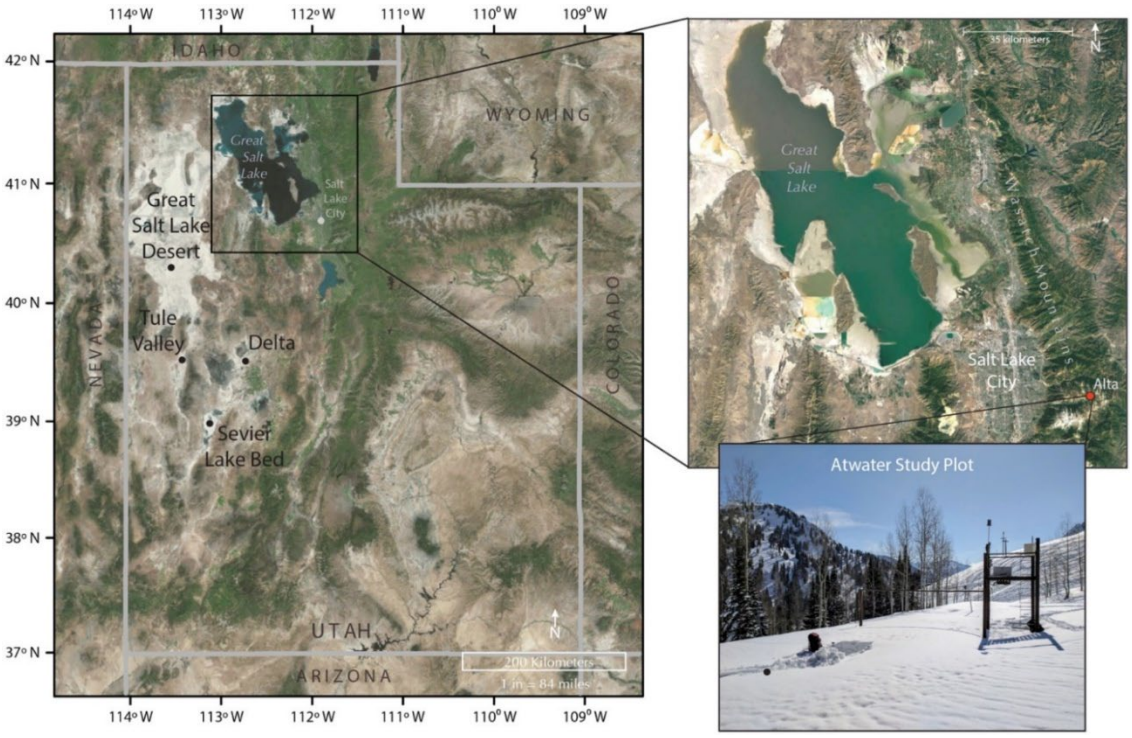

Figure 19. Nested overview map with location of commonly identified dust source regions, and location of study plot relative to Salt Lake City and the Great Salt Lake. The Atwater Study Plot instrumentation platform is shown in the inset (figure from Skiles et al., 2017).

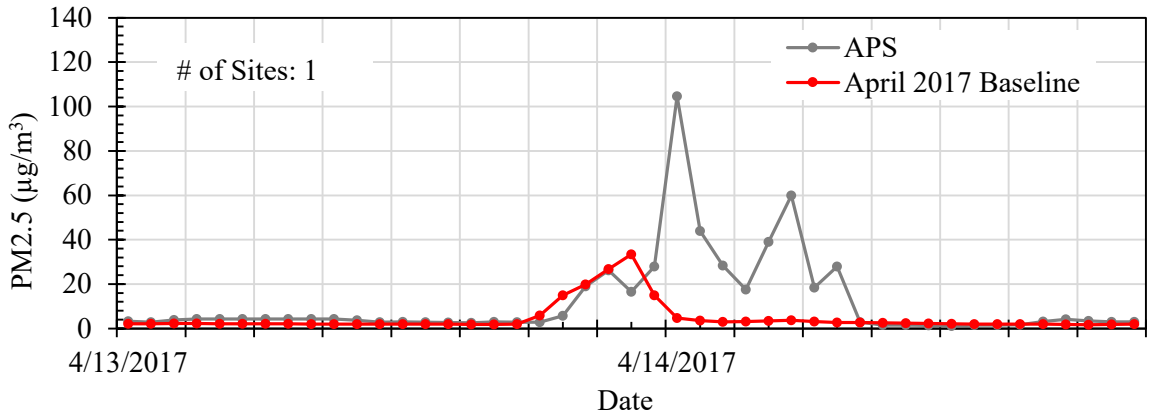

Figure 20. Baseline model results compared to Atwater Study Plot observational data (single site) for the April 13-14, 2017 dust event.

Another factor that could contribute to the differences in modeled and measured results is use of the NLCD 2011 database. While it is necessary for the Pleim-Xiu Land Surface Model (PX-LSM) and by extension the dust model in CMAQ, the NLCD 2011 database has a larger GSL than what existed in 2017. As previously noted, the NLCD 2016 has been released but has not been formatted to run with WRF at the time of this writing. As can be seen from Figure 21 the

shoreline surrounding the GSL has increased significantly since 2011. The shoreline of the GSL is an erodible source and a major producer of dust near the ASP. The increased shoreline may not be accurately represented by CMAQ, which might explain some of the discrepancy between predicted and measured dust concentration at the ASP.

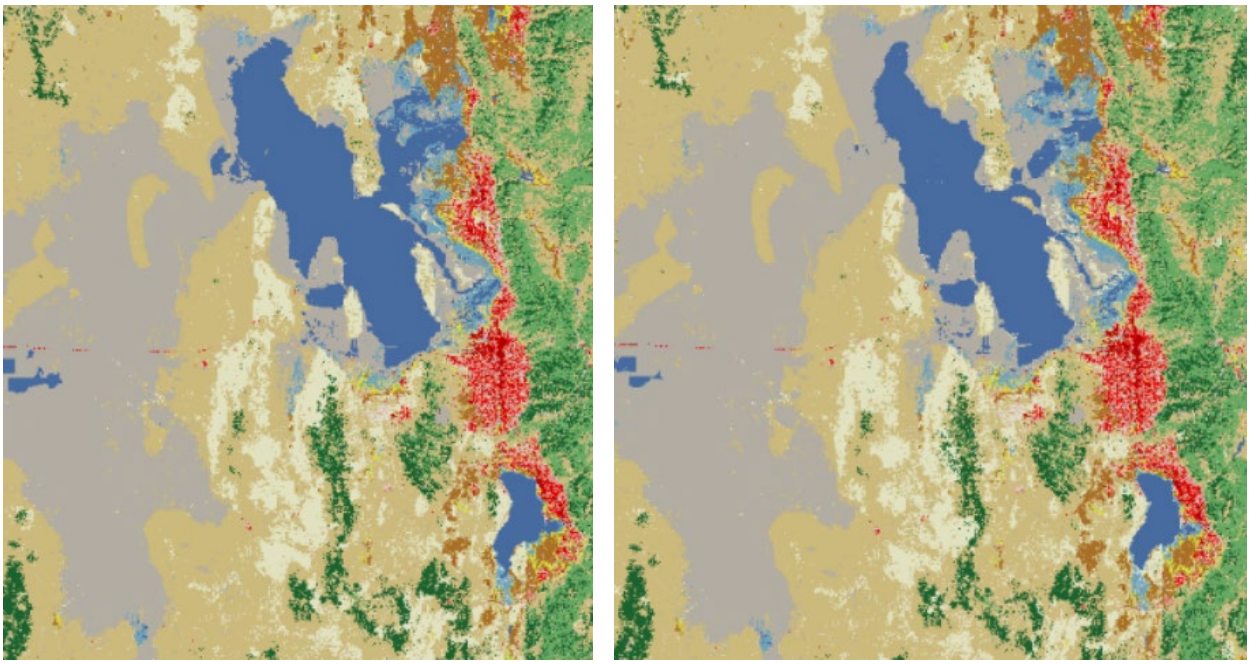

Figure 21. Comparison of the NLCD 2011 (left) and the NLCD 2016 (right) for the Great Salt Lake region. Blue represents water, gray represents barren land, tans represent at least partially vegetated areas, and red represents populated areas.

Model Grid and Time Independence

Both grid and time independence studies were performed on the model setup using the April 13-14, 2017 dust event. The grid for this study used an 8km spacing that encompassed all of Utah and the borders of surrounding states and can be seen in Figure 22. A 4km grid spacing was used with the same baseline conditions for the April case. The difference in results can be seen in Figure 23 and Figure 24. As can be seen the difference in predicted results is relatively minor, however the difference in computational cost is quite large. Both grid studies were performed using an Intel Xeon(R) Gold 6136 CPU using 40 processors. The 8km grid run took approximately 14 hours and the 4km grid took approximately 149 hours. Given the minor difference in results, the 8km grid was chosen for use with the other validation cases and future impacts scenarios.

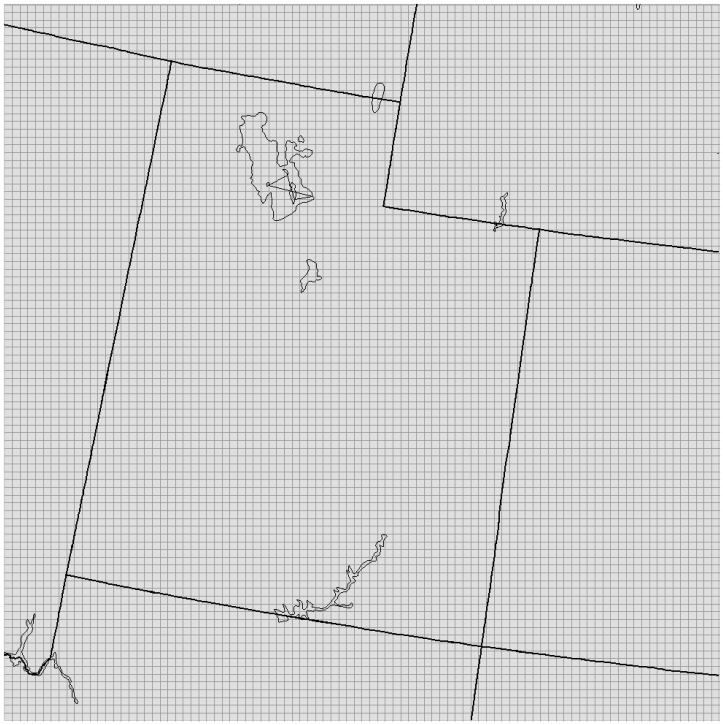

Figure 22. Computational grid used for verification and sensitivity studies. Note that state borders and major lakes in the study area have been included for reference. They do not affect the grid in any way.

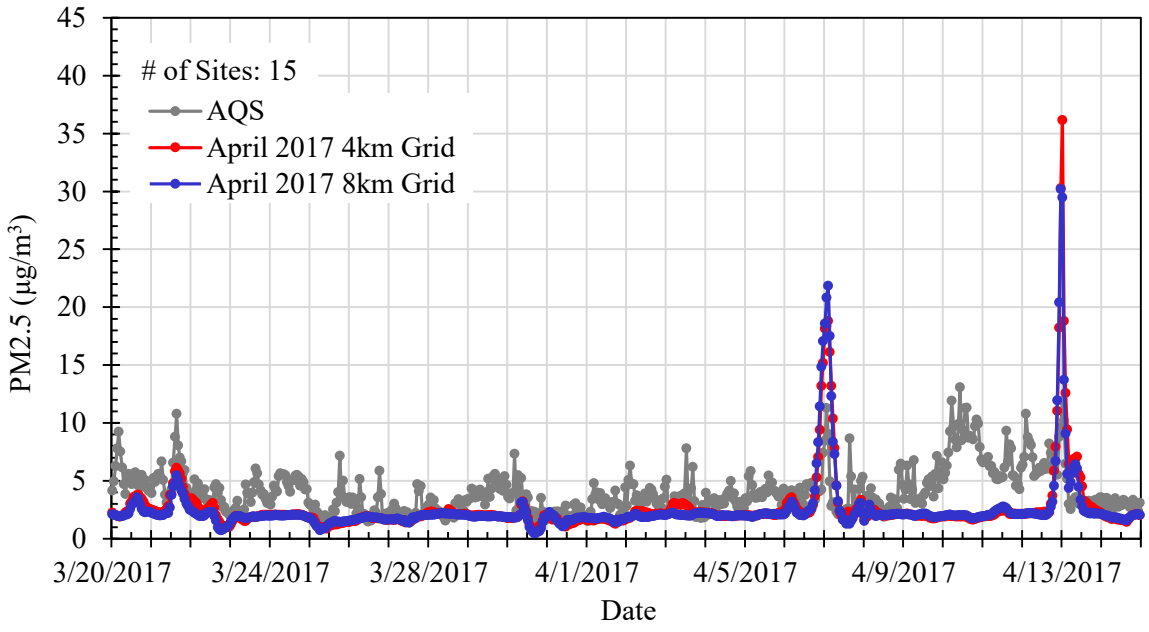

Figure 23. Comparison of the predicted results from the 8km and 4km grids using the initial month-long simulation run. Note that the number of sites used for the observations during this time period is given in the upper left corner.

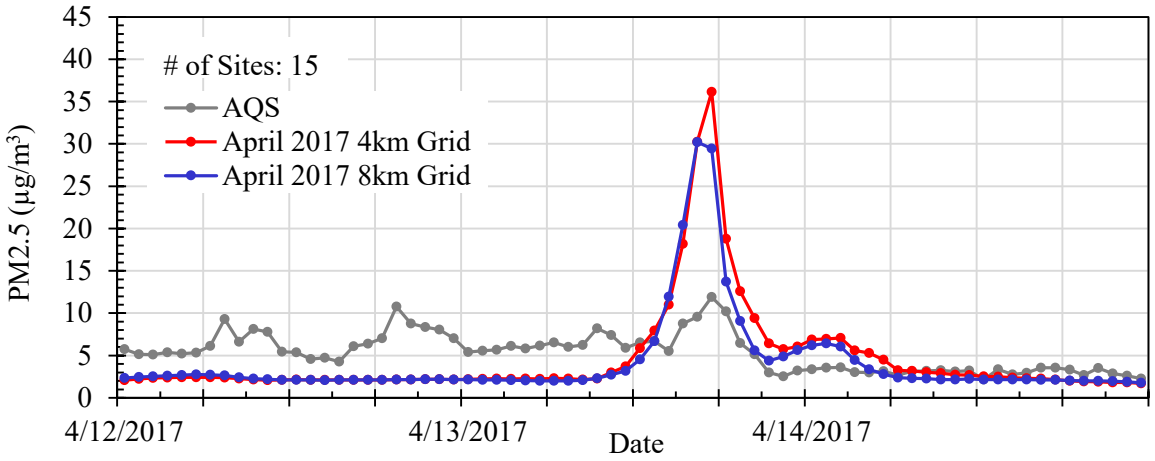

Figure 24. Comparison of the predicted results from the 8km and 4km grid focused on the April 13th dust event. Note that the number of sites used for the observations during this time period is given in the upper left corner.

As noted in the CMAQ user's guide a spin-up period is necessary prior to the beginning of the study period of interest (US EPA, 2019). Initial and boundary conditions are created using meteorological inputs from WRF and chemical profiles included in CMAQ. Spin-up periods are required by CMAQ to minimize the unwanted potential errors included in initial and boundary conditions. This is due to the transient nature of the input data. The CMAQ user guide recommends using longer spin-up periods when using chemical profiles. A time independence study was conducted to determine the impacts of the initial and boundary conditions. The study was performed by cutting the initial 30-day simulation run in half. A comparison of the 30- and 15-day simulations can be seen in Figure 25. As can be seen from the comparison, the results are virtually identical indicating time independence. Based on these results, the 15-day spin-up period was used for subsequent cases.

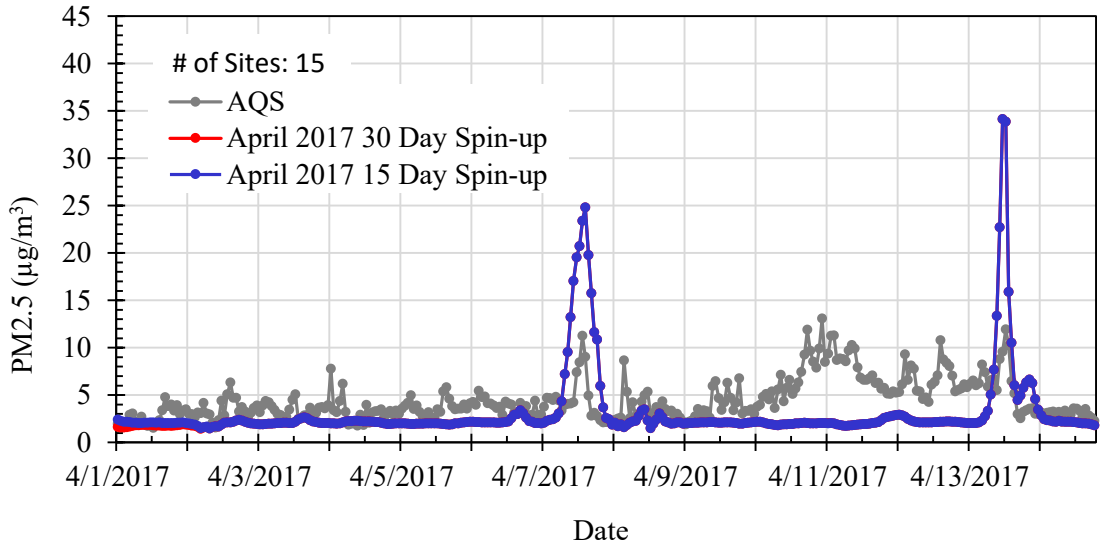

Figure 25. Comparison of 30- and 15-day simulations for the April 2017 dust event.

March 2010 Event

The March 2010 dust event comes from the paper "Wind-Blown Dust Modeling Using a Backward-Lagrangian Particle Dispersion Model" by Mallia, et al. (2017). This event was the result of a strong front moving in from the Pacific Northwest and lasted from late March 30th to early March 31st. An initial simulation was conducted from March 15th to April 1st and the results can be seen in Figure 26 and Figure 27. Figure 26 shows the results for the entire time period simulated while Figure 27 more narrowly focuses on simulation results for the time period for the dust event. Note that while the entire grid includes areas of surrounding states only data collected with monitoring stations located in Utah were used for comparisons between predicted and observed results.

As can be seen from Figure 27 the model is able to capture the timing and the relative magnitude of the event. The relatively minor differences between the modeled and observed concentrations can, like the April 2017 dust event, be attributed to error propagation or lack of resolution from meteorological fields produced by WRF. It should be noted that the model predicts a small dust event after the main dust event that doesn't occur according to the AQS network observations. This could be the result of a peripheral event that is picked up in 64 km^2 grid cell but not by the observation site.

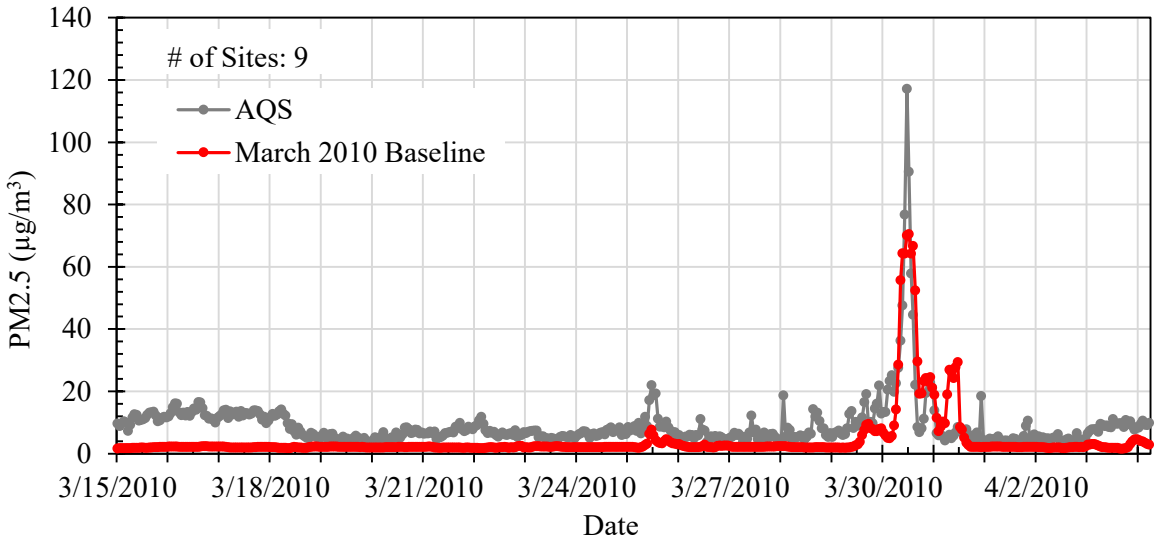

Figure 26. Baseline model results compared to observation data for the March 2010 dust event for all of Utah. Note that the number of sites used for the observations during this time period is given in the upper left corner.

The study performed by Mallia et al. included observed $PM_{2.5}$ concentrations from a site located in Salt Lake City (SLC). The observation site is the Utah Department of Environmental Quality (UDEQ) Hawthorne station (40.75° N, 111.87° W). A comparison of CMAQ results and the observed $PM_{2.5}$ concentrations is given in Figure 28.

The model predicts an earlier timing for the dust event and underpredicts the magnitude of dust observed by the Hawthorne station. The Hawthorne station is in the heart of SLC where it is difficult to accurately model meteorological conditions on an 8 km grid. Normally, WRF uses a

single layer urban canopy model to model the effects of an urban heat island, wind profile in the canopy layer, and multi-layer heat transfer (Tewan, et el., 2007). However, the Pleim-Xiu Land Surface Model (PX-LSM) required for the dust model does not include an urban canopy model so it is less accurate in representing the structural blockage and heating effects of urban areas. The combination of low spatial resolution, lack of urban effects, and measurement uncertainties likely contribute to the notable difference in predictions and measurements at this location.

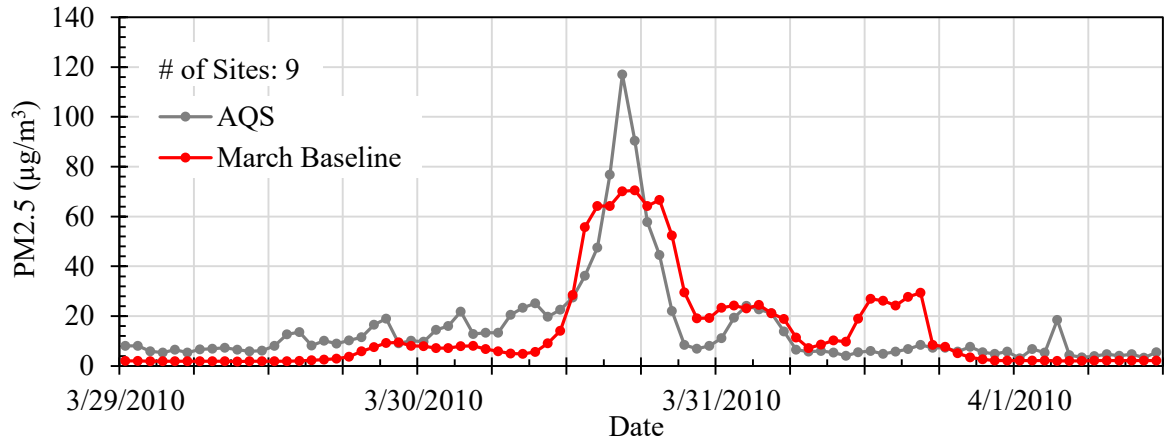

Figure 27. Baseline model results compared to observation data for the March 2010 dust event for all of Utah focused on the dust event. Note that the number of sites used for the observations during this time period is given in the upper left corner.

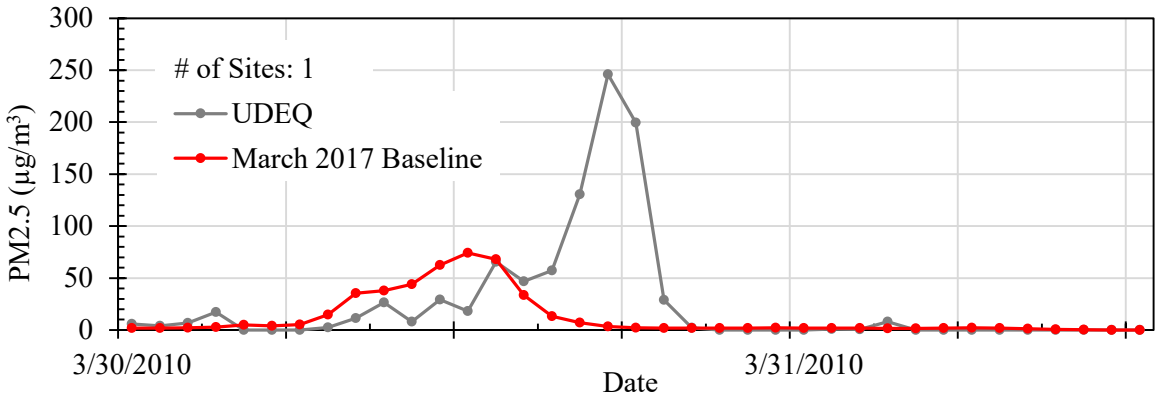

Figure 28. Comparison of model results with observed $PM_{2.5}$ concentrations at the Salt Lake City Hawthorne station (single site).

3.3.3 Model Verification with Isotopic Measurements

In addition to comparisons with dust events previously reported in the literature, predicted dust concentrations and transport patterns were also compared with dust samples collected during dust events. Two such comparisons will be reported here. The first is from August 2009 (Salt Lake City), the second is from September 2020 (Provo). Both events resulted in relatively high PM mass on the corresponding filters.

August 2009 Event

A $PM_{2.5}$ filter sample from Hawthorne Elementary School in Salt Lake City was collected on August 7, 2009, by DAQ. This sample, among others, was analyzed during this research and found to contain a significant mass of dust, suggesting a dust event may have occurred on this day. Our analysis showed a relatively high $^{87}Sr/^{86}Sr$ ratio of 0.71217 (Figure 7), suggesting that a fraction of dust originated from the dry lakebed of Great Salt Lake with high $^{87}Sr/^{86}Sr$ ratios (Figure 5). Dust modeling was conducted for this period to compare predicted dust behavior with the sample analysis. Figure 29 shows the predicted 10-m wind patterns for the period from August 7, 2009, 00:00 UTC to 03:00 UTC (local time August 6, 18:00-21:00). At 0:00 UTC, the flow is predominantly from southwest to the northeast across the state. However, a storm front from the northwest pushes this main flow from west to east across the state. This is illustrated by the wind velocity barbs west of the GSL during the 0:00 to 3:00 UTC times. The highest velocities occur at 1:00 UTC, west of the GSL.

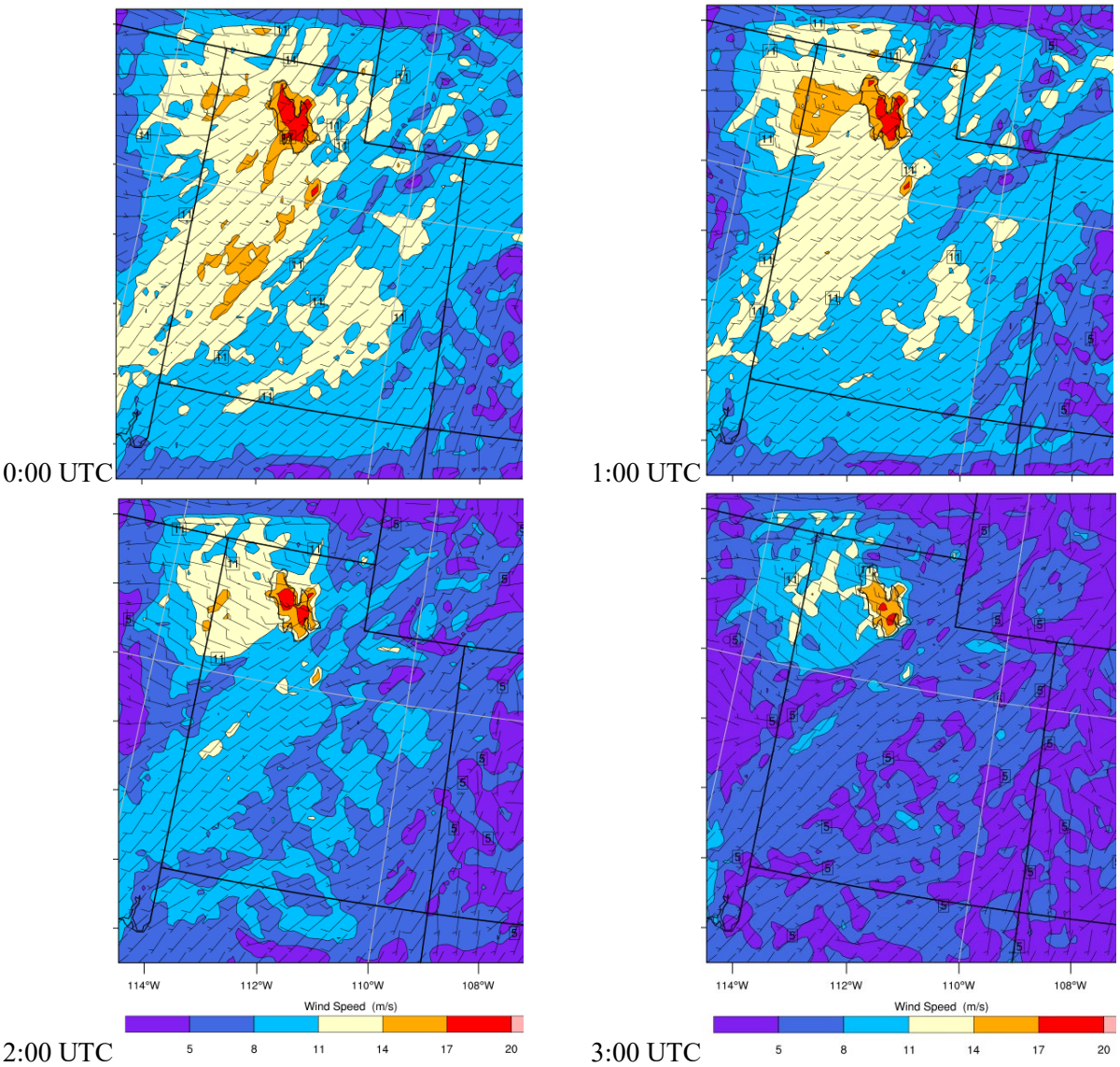

Figure 29. Wind speed profiles during the August 7, 2009 dust event from 00:00 UTC to 3:00 UTC.

This weather pattern resulted in the predicted dust emissions and transport patterns shown in Figure 30. The plotted dust concentrations from August 7, 2009 indicate a moderate pattern of dust emission and transport from the Sevier Dry Lake region as part of the southwest to northeast flow. However, as the storm front moves in from the northwest, notable dust emission occurs in the Great Salt Lake desert and is carried eastward into the SLC metro area (in the region of the Hawthorne Elementary sample site). Highest dust emissions are at 1:00 UTC, consistent with highest wind velocities. These predictions suggest notable dust emissions occurred on August 7, 2009 and that these emissions primarily originated from the GSLD and were transported eastward to SLC. These modeling results agree with the sample analysis and illustrate model accuracy in predicting correct trends in dust origins and transport. The filter sample was collected over a 24-hr period on August 7 (local time), capturing only the tail end of the dust event. Thus, the filter represents a mixture of dust from multiple sources including GSLD.

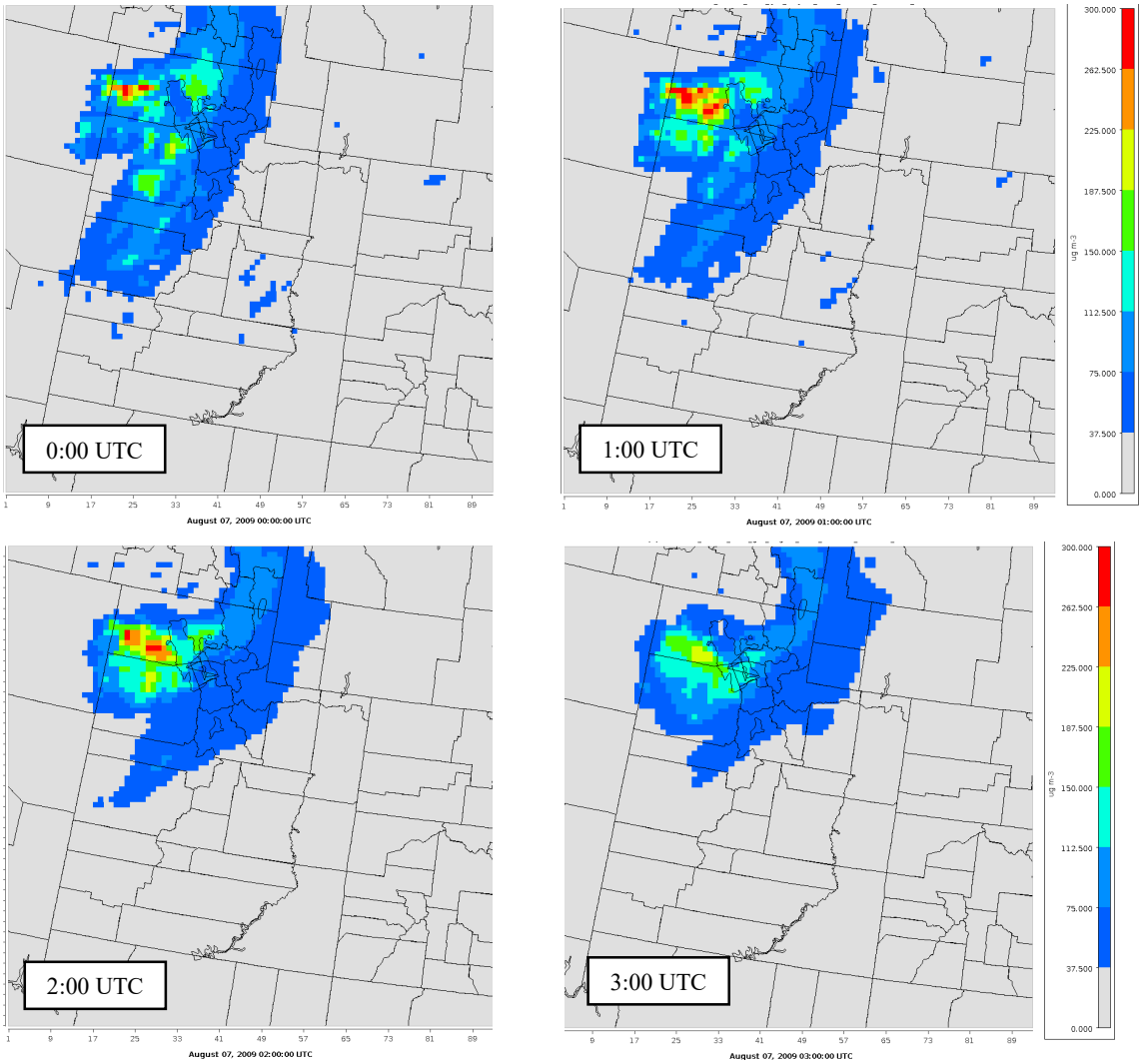

Figure 30. Modeled dust concentrations during the August 7, 2009 dust event (0:00 – 3:00 UTC) (local time August 6, 18:00-21:00). Predictions show smaller amounts of dust originating from the Sevier Dry Lake region (carried southwest to northeast) and greater amounts originating from the Great Salt Lake Desert (carried east). Dust concentration scale is 0 – 300 µg/m^3.

September 2020 Event

Observations noted a dust event in Utah on September 8th, 2020. Analysis of dust collection filters from a monitoring station at Brigham Young University (BYU) in Provo, Utah showed a relatively high $^{87}Sr/^{86}Sr$ ratio of 0.71115 in the TSP filter over the period August 26 – September 9, 2020, suggesting dust inputs from the dry lakebed of Great Salt Lake (Figure 6). The filter captured the dust event on September 8th but was also a mixture of dust from a variety of sources over the two-week period. Modeling was conducted for this same period to determine if predicted dust concentration patterns indicated dust emission origins consistent with areas identified in the filter analysis.

Figure 31 shows predicted wind patterns during this period, from 6:00 to 12:00 UTC. The top row of plots are 10-m wind velocities, which correlate with dust emission, and the bottom row of plots are 600 mbar wind velocities, which correlate with high level dust transport. The 10-m wind velocity plot at 6:00 UTC shows highest wind velocities north and west of the GSL, moving predominantly north to south. The prevailing 600 mbar wind velocities at this time are predominantly west to east across the state. These wind profiles can be compared to dust concentration profiles at similar time shown in Figure 32. The highest dust concentrations at 6:00 UTC match the location of the highest 10-m wind velocities, and occur in a north-south band west of the GSL. There are some lower dust concentrations in the center of the state, south of Utah Lake, which could be carried to that region by the higher elevation (600 mbar) west-to-east wind velocities. At 9:00 UTC, the highest 10-m wind velocities are northwest of the GSL and farther south near the Sevier Dry Lake. Similarly, the highest dust concentrations are located in the west-central part of the state, with peak concentrations near the Sevier Dry Lake. The higher elevation winds at this time have changed to more north-to-south in the northwestern part of the state, while remaining predominantly west-to-east in the central and southern parts of the state. This pattern contributes to the dispersion of the dust concentrations. Lastly at 12:00 UTC, the highest 10-m wind velocities continue to be along the western edge of the state, along with a few patches over the GSL, Wasatch Front, and southeastern Utah. The dust concentrations at this time are focused in southwestern Utah, with some regions in central and southeastern Utah. This is consistent with the location of the highest 10-m wind velocities (except over the GSL and Wasatch Front which do not have dust emission sources), where more dust is originating, and the higher elevation wind velocities which are moving in a large "L" shape along the western and southern parts of the state (north-to-south along the western boundary and west-to-east along the southern boundary), which are spreading the dust across the lower part of the state.

Results shown in Figure 32 at 6:00 UTC and 9:00 UTC show that dust originates in the GSLD and then moves south and fans out toward the east, including lower concentrations near the sample site in Provo, just east of Utah Lake. Model predictions of dust origins in the GSL desert are consistent with what is indicated by the dust collection filters at BYU, suggesting the model is capable of accurately representing the location of dust emission and direction of dust transport during major dust events.

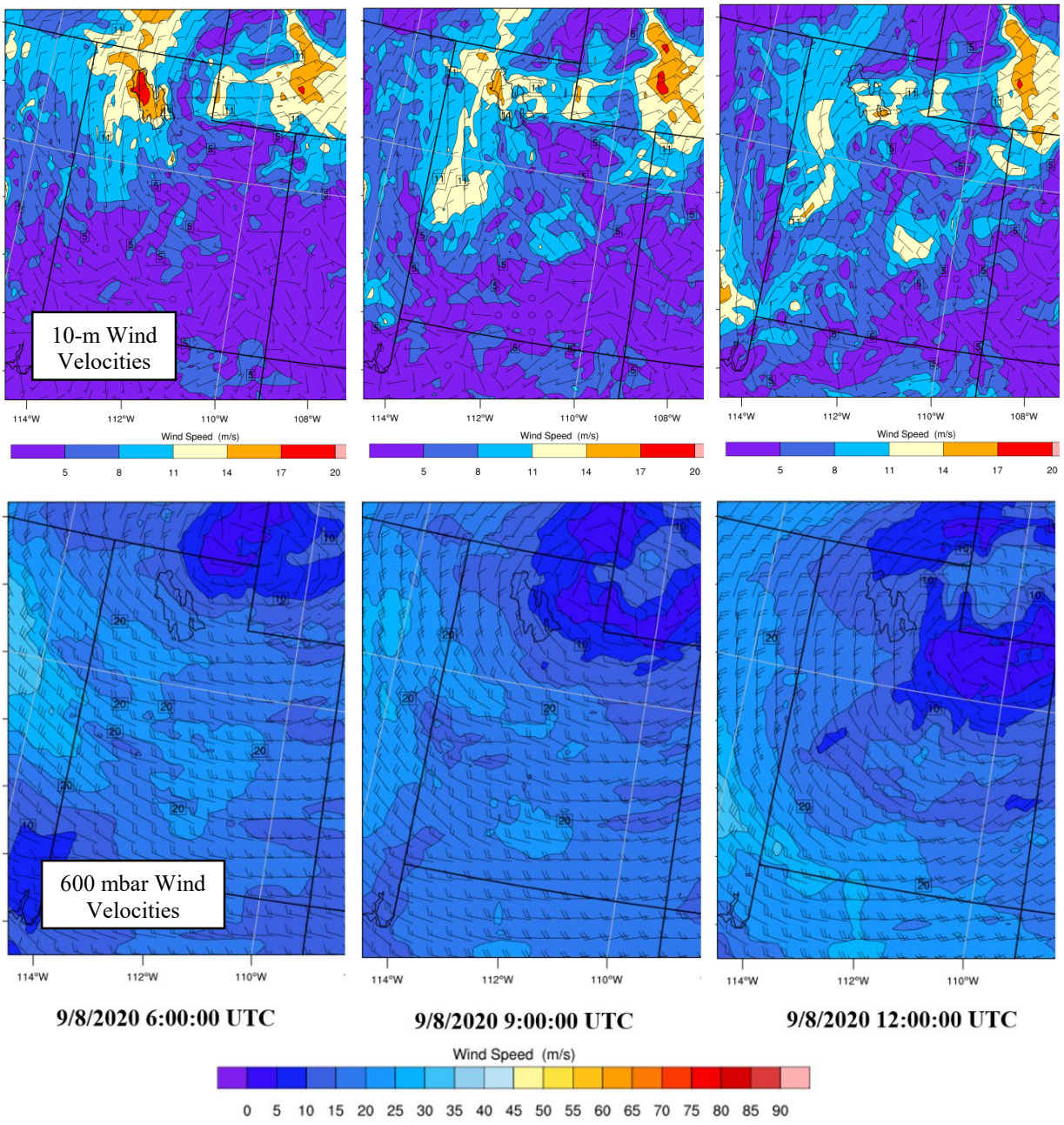

Figure 31. Wind speed profiles during the September 8, 2020 dust event. Top row are 10-m wind velocities. Bottom row are 600 mbar wind velocities. Wind conditions are shown for peak dust event hours. Wind barbs use standard wind barb notation. Wind direction is given by following the shaft from feather to tip. Wind speed is shown in meters per second via color maps for the respective wind elevations (10-m velocity range is 0-20 m/s, 600 mbar velocity range is 0-90 m/s).

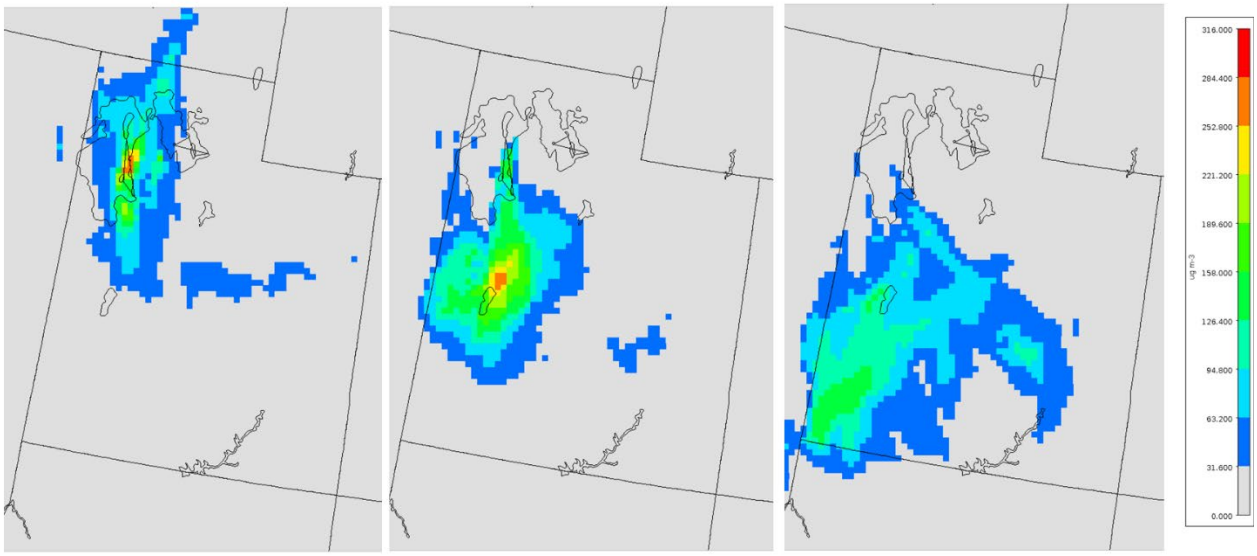

Figure 32. Modeled dust concentrations during the September 8, 2020 dust event. Model predictions show the dust originating in the Great Salt Lake Desert and Sevier Dry Lake area, and moving south and somewhat east following the prevailing wind conditions. Dust concentration scale is 0 – 316 µg/m^3.

3.4 Task 4 – Evaluate Dust Impact Scenarios

The objective of this task was to use the dust model to predict impacts of future changes to land use types on Wasatch Front dust concentrations. Such "what-if" studies can include impacts of increased or decreased dry lake shore from water management strategies, conversion of farmland to industrial sites, and siting of high-dust sources in populated areas. Such information can help guide water management and land use policies.

Two future impact studies were performed. The first was to shrink the Great Salt Lake (GSL) exposing more dry lake bed and the second was to add multiple large-scale solar farms in solar energy zones (SEZs) defined in the State of Utah. To create or modify dust emission sources (i.e., land use types), WRF output files are modified to introduce new land use types, soil properties, soil moisture, and vegetation heights. This is done by using the read_wrf_nc.exe WRF post-processing utility that modifies WRF output variable values (WRF, 2021).

A baseline for each of the future impact studies was established using the April 2017 dust event meteorology described and verified in Section 3.3.2. The reason for this was that 2017 event has more monitoring stations than that of the March 2010 dust event described in the same section. The additional monitoring stations will be able to show wider impacts of the changes made for each future impact scenario. Unfortunately, even with the additional 2017 sampling sites there are no sites close to the areas of land use changes, so visualizations created with VERDI will be used to compare local impacts of the changes in addition to comparisons at the AQS sites.

3.4.1 Shrinking Great Salt Lake

As previously discussed, the dry lakebed of Great Salt Lake (GSL) is a major dust producer. With the reduction of water levels, more dry lake bed is exposed. Future diversions and droughts will likely reduce water levels which will in turn increase the amount of erodible soil and dust emissions. Predicting the impacts of the shrinking lake on dust events can help guide water policies and lake management.

The read_wrf_nc.exe WRF post-processing utility was used to "shrink" the GSL by modifying the land water mask, soil type, soil moisture content, and vegetation height. Modifying these parameters turned the newly exposed lakebed into an area with similar conditions to the GSLD. The comparison between the baseline conditions and the shrunken GSL conditions can be seen in Figure 33.

The GSL was shrunk by 70 percent for the future impact scenario. It should be noted that the baseline size of the GSL was taken from 2011 due to the use of the 2011 National Land Cover Database (NLCD) required by the Pleim-Xiu Land Surface Model (PX-LSM). The 2011 GSL is larger than the current size of the GSL. The 70 percent reduction includes changes between 2011 and current conditions as well as assumed future reductions of 50-60 percent.

Figure 34 shows that shrinking the GSL produces only a moderate increase in dust concentrations, approximately 15 percent at peak conditions, according to the average concentrations across all AQS monitoring sites. Because of weather conditions, the monitoring stations along the Wasatch Front are only capturing the edges of the dust storm which is why there is not a greater increase in dust concentrations. However, looking at the areas surrounding the GSL through VERDI images shows that local dust concentrations are increased more (see Figure 35). Figure 36 shows the difference in concentrations between the shrinking GSL future

impact study and the baseline April 2017 dust event results for the local area surrounding the GSL. This area is shown by the red box in Figure 35. The greatest difference in dust concentrations was found to be 22 µg/m^3 or a 16.8 percent increase. For reference, the EPA 24-hour standard for $PM_{2.5}$ is 35 µg/m^3 (UDEQ, 2021). Therefore, increases in dust concentrations of this magnitude from a shrinking GSL are significant and might put Utah at risk for violating this standard in the future.

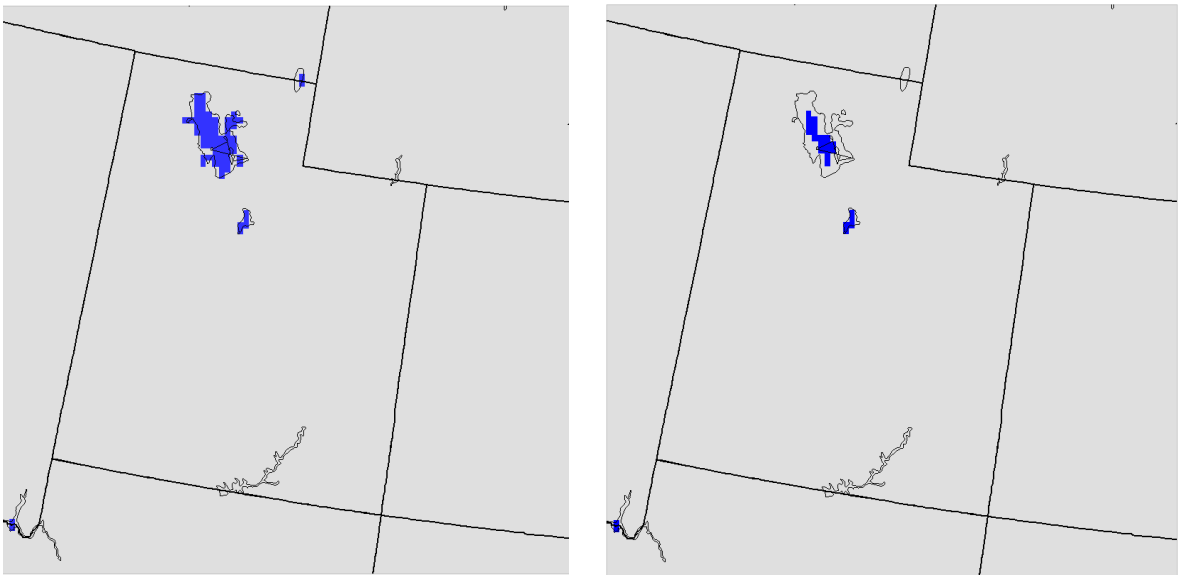

Figure 33. Comparison of the baseline size of the Great Salt Lake (left) and the shrunken Great Salt Lake (right). The Great Salt Lake is denoted by the grey squares.

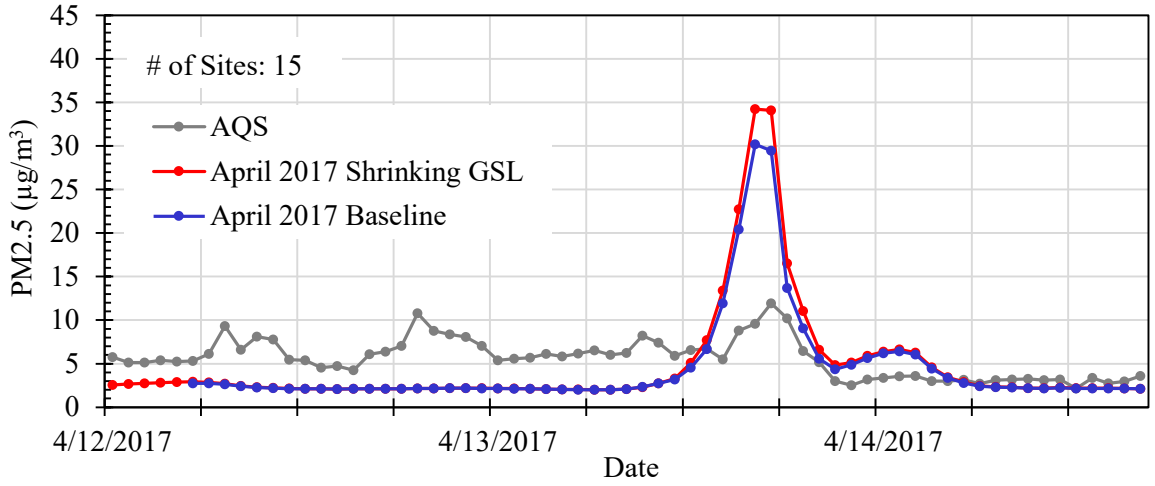

Figure 34. Comparison of observed data and modeled results where the 2011 Great Salt Lake was shrunk by 70 percent. Note that the number of sites used for the observations during this time period is given in the upper left corner.

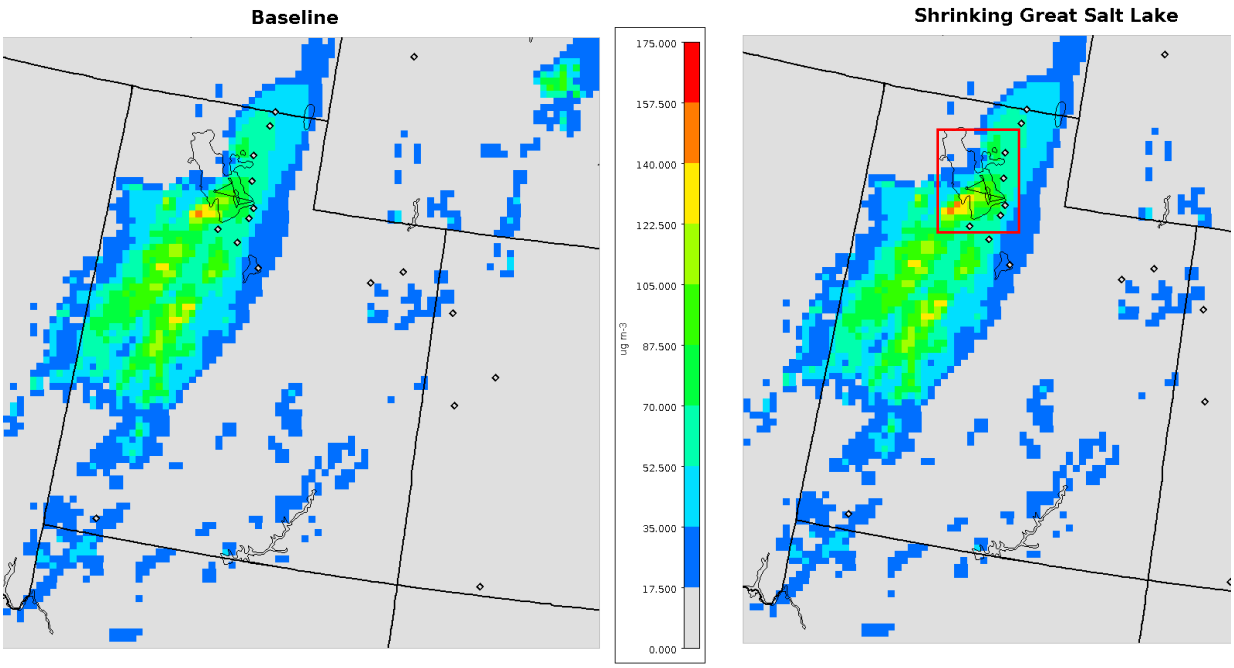

Figure 35. Comparison of modeled dust concentration results (0-175 µg/m^3) from the baseline case (left) and the modified case with the Great Salt Lake shrunken (right). The red box in the right most figure shows the area of interest for Figure 36.

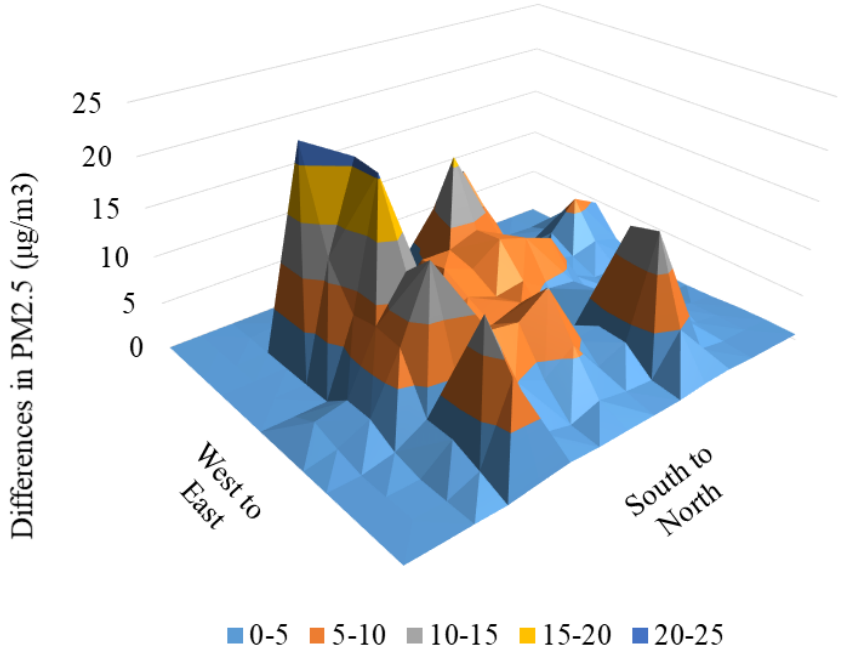

Figure 36. $PM_{2.5}$ concentration differences between the shrinking GSL future impact study and the baseline April 2017 dust event results. The specific area showing these differences is located by the red box in Figure 35.

It is important to note that if weather conditions were oriented more easterly, like the March 2010 dust event, then dust concentrations likely would be greatly increased in populated areas as the main flow pattern would carry the high local dust concentrations from the playa around the GSL directly east into the Salt Lake City area. Stronger winds would likely increase dust concentrations further than those shown in this impact study.

3.4.2 Large Scale Solar Farms

New dust sources can also be created through the construction of solar farms. As described in a technical report created for the National Renewable Energy Laboratory, "construction activities at many utility-scale ground-mounted solar installations often include clearing and grubbing of soil and roots, topsoil stripping and stockpiling, land grading and leveling, and soil compaction. Existing vegetation that supports habitat is removed and any other vegetation is often discouraged; weeds and other unwanted vegetation are generally managed with herbicides and by covering the ground with gravel (Beatty et al., 2017). Destruction of the existing vegetation and soil can lead to dust production. Currently there are several operating solar farms in Utah with many new solar farms being planned. Locations of these current and planned solar farms in Utah can be seen in Figure 37, including three Solar Energy Zones (SEZ).

To model these effects and perform predictive future impact scenarios, soil type and vegetation heights were modified using the read_wrf_nc.exe WRF post-processing utility to simulate the development of new solar farms. Large solar farms were placed in the model at Skull Valley, next to Grantsville, next to Fairfield, and on the Milford Flats South SEZ. These are large areas near population centers (other than Milford Flats) that will be good to assess the effects of solar farm emissions on populated areas. The geographical setup of this scenario can be seen in Figure 38. Each location has modified vegetation height, soil moisture, and soil types that mimic those found in the Great Salt Lake Desert (GLSD).

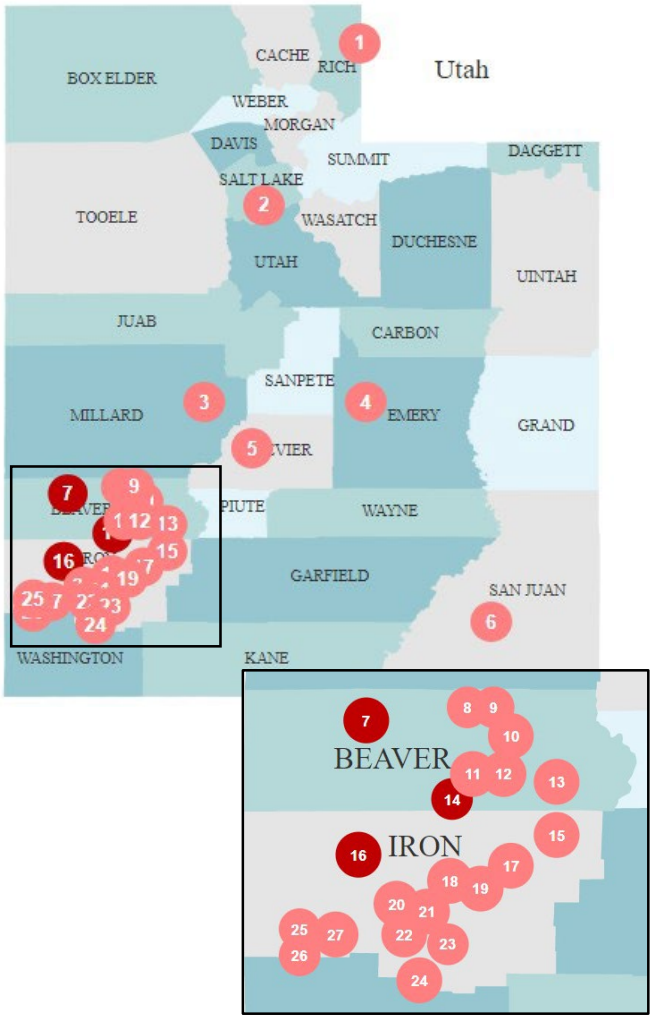

1. Sage Solar
2. Rio Tinto Stadium Array, 0.0125 km^2
3. Pavant Solar Project, 1.696 km^2
4. Hunter Solar Project, 2.31 km^2
5. Sigurd Solar, 2.43 km^2
6. Natural Bridges National Monument, 0.004 km^2
7. Wah Wah Valley SEZ, 23.8 km^2
8. Milford 1 Solar Farm, 3.02 km^2
9. Escalante Solar Project, 7.69 km^2
10. Granite Peak
11. Laho
12. Milford Flat
13. Greenville
14. Milford Flats South SEZ, 25.3 km^2
15. Buckhorn
16. Escalante Valley SEZ, 26.4 km^2
17. Red Hills Renewable Energy Park, 2.56 km^2
18. Three Peaks Solar Facility, 2.99 km^2
19. Cedar Valley
20. Granite Mountain West
21. Granite Mountain East
22. Fiddlers Canyon Solar Project, 2.56 km^2
23. Iron Springs
24. Quichapa Solar Project, 0.65 km^2
25. Cove Mountain, 4.88 km^2
26. Beryl
27. Enterprise Solar Farm, 2.63 km^2

Figure 37. Current and planned solar farms in Utah. The light red circles represent solar farms while the dark red circles represent solar energy zones (SEZ).

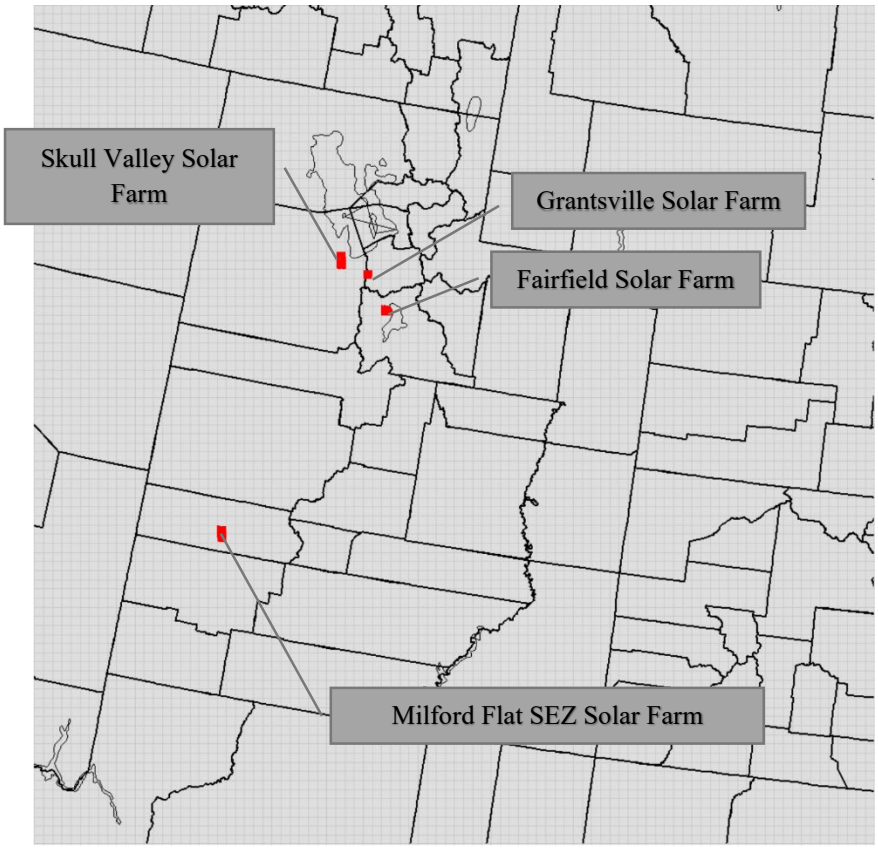

Figure 38. Locations of solar farms added to model for future impact scenario.

As can be seen from the results in Figure 39 and Figure 40, the solar farms added to the dust production found in Utah. As can be seen in Figure 39, a moderate increase in dust was seen averaged across monitoring sites. The peak dust concentration for the monitoring stations was increased by 14 percent. Dust concentrations in the surrounding areas of the added solar farms were also increased. Each of these areas analyzed are shown by the red boxes in Figure 40. The areas around the added Milford Flat SEZ Solar Farm experienced experience a 38 µg/m3 increase in peak dust concentration or a 243 percent increase. The areas around the Skull Valley and Grantsville solar farms experienced a 20 µg/m3 increase in peak dust concentration or a 20 percent increase. Figure 41 shows the differences in $PM_{2.5}$ concentrations between the April 2017 baseline model and the large-scale solar farm scenario for the area surrounding the Skull Valley and Grantsville solar farms. The increase in dust concentrations is primarily in the northwestern corner of the area. This makes sense given the wind direction during the dust event. The area around the Fairfield solar farm experienced negligible change. The lack of change in the surrounding areas of the Fairfield solar farm is most likely due to lower wind speeds in that area. Given that these additional solar farms are larger than those currently in Utah and are using idealized conditions for dust production it can be inferred that the addition of future solar farms will be of minimal impact to the Utah, except in locations immediately adjacent to the installations.

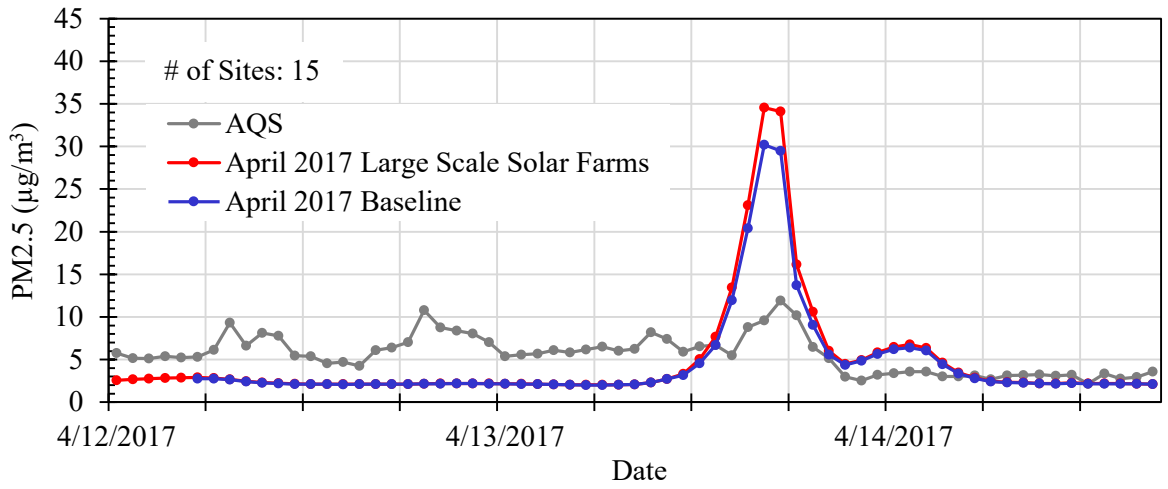

Figure 39. Comparison of observed data and modeled results where large solar farms were added in multiple locations. Note that the number of sites used for the observations during this time period is given in the upper left corner.

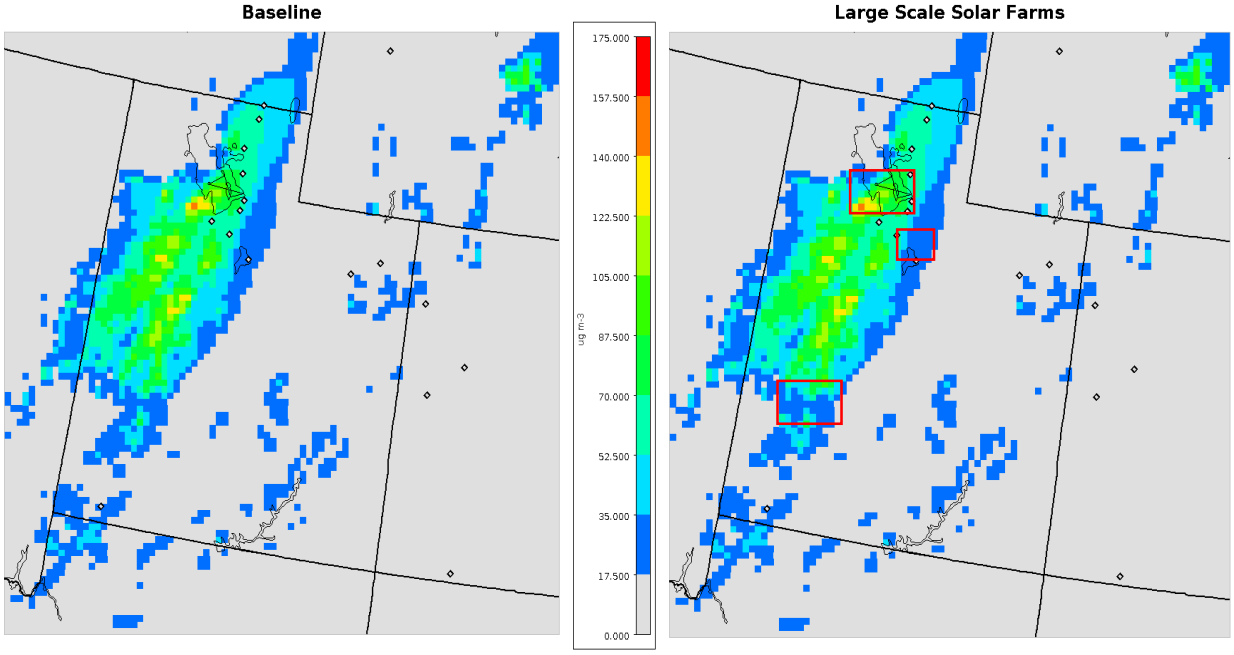

Figure 40. Comparison of modeled results from the baseline case (left) and the modified case with additional solar farms (right). Areas where solar farms were added have been outlined in red for easier comparison.

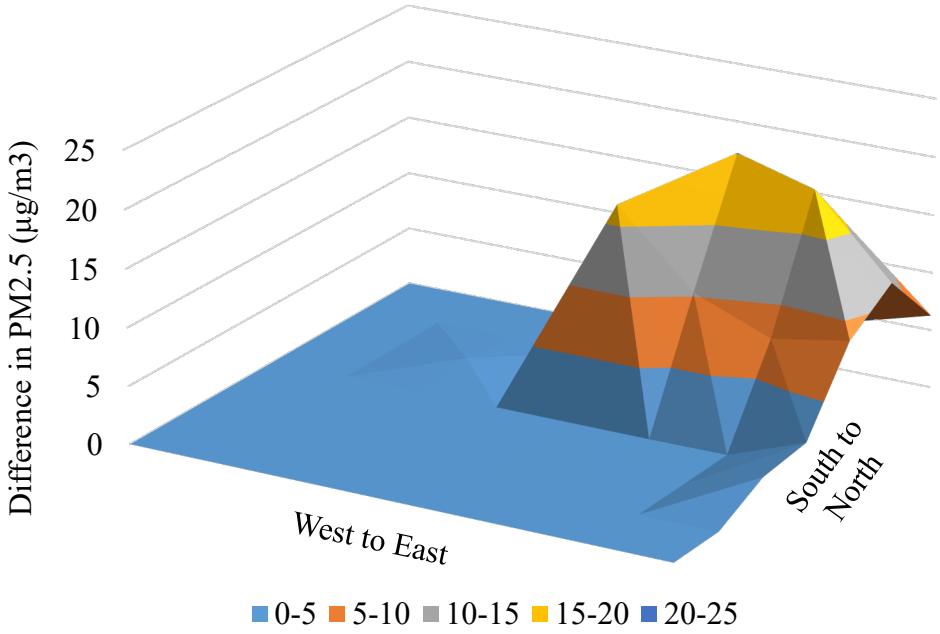

Figure 41. $PM_{2.5}$ concentration differences between the large-scale solar farm future impact study and the baseline April 2017 dust event results for the areas surrounding the Skull Valley and Grantsville Solar Farms. This area is shown by the topmost red box in Figure 40. Note the increase in dust concentrations in the northeast corner where the winds are going.

Different weather conditions could cause more significant dust production or transport dust in different directions, however, based on the weather conditions of the April 2017 event these changes would be modest. As shown in Figure 37 most planned solar farms or SEZs are located in southwestern Utah. The April 2017 dust event as shown in Figure 40 show the winds going from southwestern Utah all the way to northern Utah. These "worst case" weather conditions would produce and transport the most dust from solar farms that would reach into populated areas in northern Utah (where the observation sites are congregated). Since the solar farm contributions are so low, it is unlikely these installations will impact dust concentrations along the Wasatch Front.

These two scenarios illustrate how the dust modeling tool can be used to assess impacts of future land use changes on dust concentrations along the Wasatch Front.

4. Deviations

We were unable to obtain filters from our collaborator at Westminster College. Instead, we made measurements of TSP in addition to $PM_{2.5}$ and PM_{10} measurements at Provo. We were able to make $^{87}Sr/^{86}Sr$ measurements on nearly all of our filters, instead of the ~50 that we had expected to measure.

The future impact scenario modeling the expansion of a gravel pit near the Salt Lake – Utah County line was changed to the solar farm impacts study due to challenges in resolving the small spatial resolution of the gravel pit.

5. Major Outcomes

The major outcomes of the study are described under the four main objectives described in the subsections below.

Objective 1: Demonstrate differences between PM emissions from background sources and exceptional events using chemical signatures

We used trace and major element concentrations to demonstrate differences between exceptional events and background sources. The measurements were made on existing PM_{10} filters from UDAQ during 2008–2009 and new PM samples collected at Provo during 2019–2020. The main findings include:

- A dust event in March 2020 was characterized by elevated concentrations of Ca, Li, Mg, Na, Sr, U, V, and Zn (Figure 1). These elements are typically contained in playa-type minerals common in northern Utah dust.
- Winter periods during 2019 and 2020 had the highest concentrations of trace elements As, Cd, Fe, Mo, Pb, and Tl (Figure 2). These elements are associated with urban air pollution in northern Utah during winter inversions. The highest concentrations were typically found in the $PM_{2.5}$ fraction, supporting the idea of fine-particle urban pollution. Similar trends were found in the UDAQ PM_{10} filters collected at Salt Lake City during 2008-2009, suggesting that these elements are commonly elevated during winter across the Wasatch Front.
- Periods of firework smoke in July had elevated concentrations of B, Co, Cr, Cu, K, and Sr (Figure 3). Some of these elements also showed elevated concentrations during January from New Year's fireworks. These elements were elevated in the Provo and Salt Lake City filters during July across multiple years.

Objective 2: Identify dust source locations using isotopic "fingerprints"

We used strontium isotope ($^{87}Sr/^{86}Sr$) ratios to identify PM sources to the Wasatch Front. The measurements were made on existing PM_{10} filters from UDAQ during 2008–2009 and new PM samples collected at Provo during 2019–2020. The main findings include:

- In our Provo samples, the $^{87}Sr/^{86}Sr$ ratios varied throughout the study period, with values ranging from 0.708 to 0.712 (Figure 6). Most samples were within a narrow range of 0.709 to 0.710, which may be considered a background value for regional dust. Specifically, these values suggest inputs from Sevier Dry Lake dust throughout much of

the study period. The elevated values during spring and fall of 2020 suggest dust inputs from Great Salt Lake. The lower values during July 2019, January 2020, and July 2020 are likely Sr-rich particles from firework smoke.

- In the Salt Lake City samples, the $^{87}Sr/^{86}Sr$ ratios ranged from 0.709 to 0.715 (Figure 7). Most of the values ranged between 0.710 to 0.712, higher than values measured at Provo. The higher values likely reflect dust inputs from Great Salt Lake, a prominent dust source with a high $^{87}Sr/^{86}Sr$ ratio. The lowest $^{87}Sr/^{86}Sr$ ratio was from July 2009, reflecting Sr inputs from firework smoke. The lowest values from Provo and Salt Lake City were all measured during July, indicating an important Sr contribution from firework smoke across the Wasatch Front.

Objective 3: Develop a dust modeling framework that is validated by published studies and isotopic data

A Utah-specific dust emission and transport model was developed using WRF v4.2.1, CMAQ v5.3.1, and additional utility programs and property data. Visualization and comparison of model results to observations was accomplished using VERDI and AMET. Predicted dust concentrations were compared with AQS $PM_{2.5}$ concentrations for 2017 and 2010 dust events described in the literature (Skiles, et al., 2018; Mallia, et al. 2017). Default dust model settings were used for both predictions. The predicted peak $PM_{2.5}$ concentrations for the 2017 event were approximately double the peak AQS averages, but the timing of the peak concentration was correct. The predicted peak $PM_{2.5}$ concentrations for the 2010 event were approximately 65% the peak AQS averages, but the timing of the peak concentration was again correct. Model sensitivity studies showed additional refinement in soil properties and dust flux parameters in the model could improve model predictions.

Dust events from 2009 and 2020 were modeled to compare dust emission origins with geologic markers from filter measurements. The 2009 filter data over a 24-hour period showed a mixture of dust from multiple sources including the GSL desert. This agreed with model predictions which showed early emissions from the Sevier Dry Lake area being transported northward, followed by stronger emissions originating from the Great Salt Lake desert which were transported eastward to SLC. TSP filter data collected at BYU over the period August 26 – September 9, 2020 suggested dust emissions from the dry lakebed of Great Salt Lake. This was consistent with a strong weather pattern on September 8 moving eastward across the GSL which was predicted to produce significant dust emissions that were transported to SLC. These results suggest the dust model is capable of accurately representing the location of dust emission and direction of dust transport during major dust events.

Objective 4: Use the validated dust model to predict impacts of future emissions under changing land use and climate conditions.

Future impact scenarios were performed to predict the effects of a shrinking GSL and addition of multiple solar farms in Utah. These future impact scenarios were accomplished by modifying WRF outputs using the read_wrf_nc.exe utility program and were based on the April 13-14, 2017 weather conditions. Results showed that:

- Shrinking the GSL increased the amount of dust produced during dust events. Shrinking the GSL by approximately 50-60% increased the peak dust concentration averaged across

all monitoring stations by approximately 15 percent. The peak dust concentration in the local area surrounding the GSL shoreline was increased by 22 $\mu g/m^3$. Current conservation efforts have minimized the shrinking of GSL however if these policies are reversed or significant climate change occurs then dust production will likely increase.

- The addition of multiple solar farms in Utah increased the overall dust for the April 2017 dust event. The peak dust concentration averaged across all monitoring stations was increased by 14 percent. Dust concentrations in the areas immediately surrounding these theoretical solar farms increased. The areas around the added Milford Flat SEZ Solar Farm experienced experience a 38 $\mu g/m^3$ increase in peak dust concentration. The areas around the Skull Valley and Grantsville solar farms experienced a 20 $\mu g/m^3$ increase in peak dust concentration. The area around the Fairfield solar farm experienced negligible change. This would be important to local communities who would experience the brunt of these effects but would have lesser impact on the densely populated regions along the Wasatch Front.

6. Future Direction

The observations and modeling started by Dr. Carling and Dr. Adams with this project are continuing with a five-year NSF project called DUST^2 (Dust along and Urban to Summit Transect). The project is a collaboration with dust researchers from the University of Utah, Utah State University, Salt Lake Community College, and Middlebury college to understand source-to-sink dust processes in the southwestern US (https://criticalzone.org/dust2).

As part of Dust^2, Dr. Carling is continuing to collect biweekly PM_{10} filters in Provo for chemical and isotopic measurements. With additional funding, Carling would like to analyze additional archived DAQ filters for investigations of dust events, firework pollution, and winter inversions over multiple years. Future work would further investigate chemical and isotopic signatures of these exceptional events that could be used by DAQ to identify sources of air pollution along the Wasatch Front.

Results from the modeling work illustrated two key elements for future work. First, model results illustrated model dependence on soil properties including salt concentration and surface crustiness and particle diameter (inherent in threshold friction velocity calculation). These properties are not well defined for the specific dust source regions (e.g., GSLD) around the Wasatch Front. Improved characterization of these properties should improve dust emission predictions. Fortunately, this research is currently being conducted by Dr. Kevin Perry at the University of Utah as part of Dust^2 and the results will be shared with Dr. Adams as part of his work on the same program. Second, current modeling was conducted with large computational grids (4-8 km) commonly used for this type of modeling where meteorological data and land use properties are not well resolved. However, this spatial resolution is not sufficient to capture dust events that are caused by smaller localized behavior such as gravel pits, construction sites, and livestock feed lots and loading zones. Such zones do not cause widespread dust impacts, but can significantly impact locally adjacent areas. Future work can focus on how to resolve dust events for these smaller, more focused areas. Note such increased spatial resolution could also accommodate more specific local soil properties.

Lastly, model results illustrated the relative brevity of significant dust events, which typically last only a few hours and involve strong directional winds. Filters typically collect data over a

much longer period and can dilute dust from the immediate event with dust from a longer time period (and different origins). Development of a filter that could be remotely operated to take data only during these brief dust events would allow more precise comparisons between predicted and sampled data, particularly if comparing geologic origin data. To improve the link between modeling and isotopic measurements, we propose to perform time-resolved sampling during dust events to capture dust from specific events. We would like to develop a system to collect dust on filters at an hourly time step during a dust event to capture dust from different sources as a dust storm progresses. The isotopic signatures from hourly filters would be compared with the model results to improve the accuracy of modeling results.

7. Data Management

The Appendix includes model input files for model simulation. Additional data will be posted to a public website identified by UDAQ within 8 months of project completion:

- Copies of slides from presentations at Air Quality: Science for Solutions conferences.
- A spreadsheet with trace element chemistry for 147 PM filters and Sr isotope ($^{87}Sr/^{86}Sr$) ratios for 141 PM filters.
- Summary of simulation results from the model cases. In addition to the model input files in the Appendix and the comparison graphs and color plots shown in the report, GIF files of dust concentrations for each of the four events modeled (August 2009, March 2010, April 2017, September 2020) will be posted to the website. Full WRF and CMAQ output files will not be included on the website due to their large (terabyte) size.

Bibliography

Appel, W.K., 2019. Atmospheric Model Evaluation Tool v1.4 User's Guide.

Beatty, B., J. Macknick, J. McCall and G. Braus, 2017. "Native Vegetation Performance under a Solar PV Array at the National Wind Technology Center," Golden, CO.

Cahill, T.A., Gill, T.E., Reid, J.S., Gearhart, E.A., and Gillette, D.A., 1996. Saltating particles, playa crusts and dust aerosols at Owens (dry) Lake, California. Earth Surface Processes and Landforms, 21: 621-639.

Carling, G.T. et al., 2020. Using strontium isotopes to trace dust from a drying Great Salt Lake to adjacent urban areas and mountain snowpack. Environmental Research Letters, 15(11): 114035.

Foley, 2020. "Appendix E: Configuring the Weather Research and Forecasting Model (WRF) for Use with Air Quality Models," [Online]. Available: https://github.com/USEPA/CMAQ/blob/master/DOCS/Users_Guide/Appendix/CMAQ_UG_appendixE_configuring_WRF.md.

Foroutan, H., J. Young, S. Napelenok, L. Ran, K. W. Appel, R. C. Gilliam, and J. E. Pleim, 2017. Development and evaluation of a physics-based windblown dust emission scheme implemented in the CMAQ modeling system, J. Adv. Model. Earth Syst., 9, 585–608.

Gill, TE, and DA Gillette, 1991. Owens Lake: A natural laboratory for aridification, playa desiccation and desert dust. Geological Society of America, 23: 462.

Gilliam, R., and J. Pleim, December 2015. Overview of Science Processes in CMAQ [Online]. Available: https://www2.mmm.ucar.edu/wrf/users/docs/PX-ACM.pdf. [Accessed May 2021].

Goodman, M.M., G. T. Carling, D. P. Fernandez, K. A. Rey, C. A. Hale, B. R. Bickmore, S. T. Nelson and J. S. Munroe, 2019. Trace element chemistry of atmospheric deposition along the Wasatch Front (Utah, USA) reflects regional playa dust and local urban aerosols., Chemical Geology, vol. 530, no. 0009-2541, p. 119317.

Hahnenberger, M. and Nicoll, K., 2012: Meteorological characteristics of dust storm events in the eastern Great Basin of Utah, U.S.A. Atmospheric Environment, 60(0): 601-612.

Kang, J.Y., S.-C. Yoon, Y. Shao and S.-W. Kim, 2011. "Comparison of vertical dust flux by implementing three dust emission schemes in WRF/Chem," Journal of Geophysical research: Atmospheres, vol. 116, no. D9.

Lawless, Zachary D.; Cable, Ariel S.; Van Dyke, Cameron B.; and Adams, Bradley R., 2021. "User Guide for Dust Modeling Using CMAQ 5.3.1 and WRF 4.2.1". Faculty Publications. 5515. https://scholarsarchive.byu.edu/facpub/5515.

Li, J., T. Kandakji, J. A. Lee, J. Tatarko, J. Blackwell 3rd, T. E. Gill and J. D. Collins, 2018. "Blowing dust and highway safety in the southwestern United States: Characteristics of dust emission "hotspots" and management implications," Science of the Total Environment, vol. 621, pp. 1023-1032.

Mallia, DV, A. Kochanski, D. Wu, C. Pennell, W. Oswald, J. C. Lin, 2017. Wind-Blown Dust Modeling Using a Backward-Lagrangian Particle Dispersion Model, J. Applied Meteorology and Climatology, 56:10, 2845-2867.

NCAR, 2021. National Center for Atmospheric Research Mesoscale & Microscale Meteorology Laboratory, "User's Guides for the Advanced Research WRF (ARW) Modeling System, Version 4". [Online]. Available: https://www2.mmm.ucar.edu/wrf/users/docs/user_guide_v4/contents.html.

NCEP, 2004. National Centers for Environmental Prediction, National Weather Service, NOAA, U.S. Department of Commerce, *NCEP ADP Global Surface Observational Weather Data, October 1999 - continuing*, Boulder, CO: Research Data Archive at the National Center for Atmospheric Research, Computational and Information Systems Laboratory.

NCEP, 2000. National Centers for Environmental Prediction, National Weather Service, NOAA, U.S. Department of Commerce, *NCEP FNL Operational Model Global Tropospheric Analyses, continuing from July 1999,* Research Data Archive at the National Center for Atmospheric Research, Computational and Information Systems Laboratory.

NWS, 2021. National Weather Service, "Information about wind barbs," [Online]. Available: https://www.weather.gov/hfo/windbarbinfo.

Reheis, M.C., 1997. Dust deposition downwind of Owens (dry) Lake, 1991–1994: Preliminary findings. Journal of Geophysical Research: Atmospheres 102, 25999-26008.

Reheis MC, Budahn JR, Lamothe PJ. 2002. Geochemical evidence for diversity of dust sources in the southwestern United States. Geochimica et Cosmochimica Acta 66: 1569-1587.

Reheis MC, Budahn JR, Lamothe PJ, Reynolds RL. 2009. Compositions of modern dust and surface sediments in the Desert Southwest, United States. Journal of Geophysical Research-Earth Surface 114: 20.

Shao, Y., M. Ishizuka, M. Mikami and F. Leys, 2011. "Parameterization of size-resolved dust emission and validation with measurements," Journal of Geophysical Research: Atmospheres, vol. 116, no. D8.

Skiles, S.M., Derek, V.M., Hallar, A.G., John, C.L., Andrew, L., Ross, P., Steven, C., 2018. Implications of a shrinking Great Salt Lake for dust on snow deposition in the Wasatch Mountains, UT, as informed by a source to sink case study from the 13–14 April 2017 dust event. Environmental Research Letters 13:12, 124031.

Steenburgh W, Massey JD, Painter TH. 2012. Episodic Dust Events of Utah's Wasatch Front and Adjoining Region. Journal of Applied Meteorology and Climatology 51: 1654-1669.

Tewan, M., F. Chen, H. Kusaka and S. Miao, 2007. [Online]. Available: https://ral.ucar.edu/sites/default/files/public/product-tool/WRF-LSM-Urban.pdf.

Todd, M.C., D. B. Karam, C. Cavazos, C. Bouet, B. Heinold, J. M. Baldasano, G. Cautenet, I. Koren, C. Perez, F. Solmon, I. Tegen, P. Tulet, R. Washington and A. Zakey, 2008. "Quantifying uncertainty in estimates of mineral dust flux: An intercomparison of model performance over the Bodélé Depression, northern Chad," Journal of Geophysical Research: Atmospheres, vol. 113, no. D24.

UCAR, 2021. University Corporation for Atmospheric Research, "LITTLE_R Help,". [Online]. Available: https://www2.mmm.ucar.edu/wrf/users/wrfda/OnlineTutorial/Help/littler.html.

UDEQ, 2021. Utah Department of Environmental Quality, "Particulate Matter 2.5 (PM2.5) Overview". [Online]. Available: https://deq.utah.gov/air-quality/particulate-matter-2-5-pm2-5-overview.

Uno, I., Z. Wang, M. Chiba, Y. S. Chun, S. L. Gong, Y. Hara, E. Jung, S. S. Lee, M. Liu, M. Mikami, S. Music, S. Nickovic, S. Satake, Y. Shao, N. Song, N. Sugimoto, T. Tanaka and D. L. Westphal, 2006. "Dust model intercomparison (DMIP) study over Asia: Overview," Journal of Geophysical Research: Atmospheres, vol. 111, no. D12.

USEPA, 2017 "Visual Environment for Rich Data Interpretation (VERDI) program for environmental modeling systems". [Online]. Available: https://www.epa.gov/air-research/visual-environment-rich-data-interpretation-verdi-program-environmental-modeling.

USEPA, 2019. National Exposure Research Laboratory. "CMAQ User's Guide," [Online]. Available: https://github.com/USEPA/CMAQ/blob/5.3.1/DOCS/Users_Guide/README.md.

USEPA, 2020a. "Air Quality System (AQS)" [Online]. Available: https://www.epa.gov/aqs.

USEPA, 2020b. "CMAQ: The Community Multiscale Air Quality Modeling System". [Online]. Available: https://www.epa.gov/cmaq.

USEPA, 2021a. "Overview of Science Processes in CMAQ," 4th May 2021. [Online]. Available: https://www.epa.gov/cmaq/overview-science-processes-cmaq.

USEPA, 2021b. "CMAQ User's Guide," 7 May 2021. [Online]. Available: https://github.com/USEPA/CMAQ/tree/master/DOCS/Users_Guide.

Utah Department of Environmental Quality, 2017. "Particulate Matter 2.5 (PM2.5) Overview," 7 July 2017. [Online]. Available: https://deq.utah.gov/air-quality/particulate-matter-2-5-pm2-5-overview.

Wang et al., 2018. "WRF Users Page". [Online]. Available: https://ww2.mmm.ucar.edu/wrf/users/docs/user_guide_v4/v4.2/WRFUsersGuide_v42.pdf.

Wang, W., C. Bruyere, M. Duda, J. Dudhia, D. Gill, M. Kavulich, K. Werner, M. Chen, H.-C. Lin, J. Michalakes, S. Rizvi, X. Zhang, J. Berner, D. Munoz-Esparza, B. Reen, S. Ha and K. Fossell, 2020. "User's Guides for the Advanced Research WRF (ARW) Modeling System, Version 4". [Online]. Available: https://www2.mmm.ucar.edu/wrf/users/docs/user_guide_v4/v4.2/WRFUsersGuide_v42.pdf.

WPS, 2021. "WPS V4 Geographical Static Data Downloads Page". [Online]. Available: https://www2.mmm.ucar.edu/wrf/users/download/get_sources_wps_geog.html.

WRF, 2021. Weather Research and Forecasting Model, "Utility: read_wrf_nc". [Online]. Available: https://www2.mmm.ucar.edu/wrf/OnLineTutorial/Tools/read_wrf_nc.php.

Wurtsbaugh, W.A., Miller, C., Null, S.E., DeRose, R.J., Wilcock, P., Hahnenberger, M., Howe, F., Moore, J., 2017. Decline of the world's saline lakes. Nat. Geosci. 10, 816.

Xiu A. and J. Pleim, 2001. "Development of a Land Surface Model Part I: Application in a Mesoscale Meteorological Model," Journal of Applied Meteorology, vol. 40, pp. 192-209.

Zou, X., I. M. Navon and F. X. Ledimet, 1992. "An optimal nudging data assimilation scheme using parameter," Quarterly Journal of the Royal Meteorological Society, vol. 118, pp. 1163-1186.

APPENDIX A. WRF NAMELIST.INPUT AND NAMELIST.OA FOR EACH CASE

A.1 April 2017 Dust Event

namelist.input

```
 &time_control
 run_days                            =        0
 run_hours                           =        0
 run_minutes                         =        0
 run_seconds                         =        0
 start_year                          =        2017
 start_month                         =        3
 start_day                           =        1
 start_hour                          =        12
 end_year                            =        2017
 end_month                           =        4
 end_day                             =        20
 end_hour                            =        18
 interval_seconds                    =        21600
 input_from_file                     =        .true.
 history_interval                    =        60
 frames_per_outfile                  =        1000
 restart                             =        .false.
 restart_interval                    =        7200
 io_form_history                     =        2
 io_form_restart                     =        2
 io_form_input                       =        2
 io_form_boundary                    =        2
 io_form_auxinput2                   =        2
 auxinput4_inname                    =        wrflowinp_d<domain>
 auxinput4_interval                  =        360
 io_form_auxinput4                   =        2
 auxinput11_interval                 =        1
 auxinput11_end_h                    =        99999
 force_use_old_data                  =        T
 /

 &domains
 time_step                           =        10
 time_step_fract_num                 =        0
```

```
time_step_fract_den     =       1
max_dom                 =       1
e_we                    =       95
e_sn                    =       95
e_vert                  =       33
p_top_requested         =       5000
num_metgrid_levels      =       32
num_metgrid_soil_levels =       4
dx                      =       8000
dy                      =       8000
grid_id                 =       1
parent_id               =       1
i_parent_start          =       1
j_parent_start          =       1
parent_grid_ratio       =       1
parent_time_step_ratio  =       1
feedback                =       1
smooth_option           =       0
sfcp_to_sfcp            =       .true.
/

&physics
mp_physics              =       8
cu_physics              =       6
ra_lw_physics           =       4
ra_sw_physics           =       4
bl_pbl_physics          =       7
sf_sfclay_physics       =       7
sf_surface_physics      =       7
radt                    =       30
bldt                    =       0
cudt                    =       5
icloud                  =       1
num_land_cat            =       40
num_soil_layers         =       2
sf_urban_physics        =       1
pxlsm_modis_veg         =       1
sst_update              =       1
pxlsm_smois_init        =       1
/
```

```
&fdda
pxlsm_soil_nudge        =       1
grid_fdda               =       1
gfdda_inname            =       wrffdda_d<domain>
gfdda_interval_m        =       360
gfdda_end_h             =       99999
io_form_gfdda           =       2
fgdt                    =       0
if_no_pbl_nudging_uv    =       0
if_no_pbl_nudging_t     =       1
if_no_pbl_nudging_q     =       0
if_zfac_uv              =       0
k_zfac_uv               =       10
if_zfac_t               =       0
k_zfac_t                =       10
if_zfac_q               =       0
guv                     =       0.0001
gt                      =       0.0001
gq                      =       0.00001
if_ramping              =       1
dtramp_min              =       60

grid_sfdda              =       1
sgfdda_inname           =       wrfsfdda_d<domain>
sgfdda_end_h            =       999999
sgfdda_interval_m       =       360
sgfdda_interval         =       21600
guv_sfc                 =       0
gt_sfc                  =       0
gq_sfc                  =       0
rinblw                  =       250

obs_nudge_opt           =       0
max_obs                 =       300000
fdda_start              =       0
fdda_end                =       99999
obs_nudge_wind          =       0
obs_coef_wind           =       0.0006
obs_nudge_temp          =       0
obs_coef_temp           =       0.0006
obs_nudge_mois          =       0
```

```
obs_coef_mois           =       0.0006
obs_rinxy               =       240
obs_rinsig              =       0.1
obs_twindo              =       0.66667
obs_npfi                =       10
obs_ionf                =       2
obs_idynin              =       0
obs_dtramp              =       40
obs_prt_freq            =       10
obs_prt_max             =       10
obs_ipf_errob           =       .true.
obs_ipf_nudob           =       .true.
obs_ipf_in4dob          =       .true.
/

&dynamics
hybrid_opt              =       2
w_damping               =       0
diff_opt                =       1
km_opt                  =       4
diff_6th_opt            =       0
diff_6th_factor         =       0.12
base_temp               =       290
damp_opt                =       3
zdamp                   =       5000
dampcoef                =       0.2
khdif                   =       0
kvdif                   =       0
non_hydrostatic         =       .true.
moist_adv_opt           =       1
scalar_adv_opt          =       1
gwd_opt                 =       1
epssm
/

&bdy_control
spec_bdy_width          =       5
specified               =       .true.
/

&grib2
```

```
/

 &namelist_quilt
 nio_tasks_per_group      =        0
 nio_groups               =        1
 /
```

namelist.oa

```
 &record1
 start_year                      =  2017
 start_month                     =  3
 start_day                       =  1
 start_hour                      =  12
 end_year                        =  2017
 end_month                       =  4
 end_day                         =  20
 end_hour                        =  18
 interval                        =  21600
 /

 &record2
 grid_id                         =  1
 obs_filename                    =  'SURFACE_OBS'
 remove_data_above_qc_flag       =  32768
 remove_unverified_data          =  .TRUE.
 /
 obs_filename                    =  '.'
 trim_domain                     =  .TRUE.
 trim_value                      =  5

 &record3
 max_number_of_obs               =  400000
 fatal_if_exceed_max_obs         =  .TRUE.
 /

 &record4
 qc_test_error_max               =  .TRUE.
 qc_test_buddy                   =  .FALSE.
 qc_test_vert_consistency        =  .TRUE.
 qc_test_convective_adj          =  .TRUE.
```

```
max_error_t                     =   10
max_error_uv                    =   13
max_error_z                     =   8
max_error_rh                    =   50
max_error_p                     =   600
max_buddy_t                     =   8
max_buddy_uv                    =   8
max_buddy_z                     =   8
max_buddy_rh                    =   40
max_buddy_p                     =   800
buddy_weight                    =   1
max_p_extend_t                  =   1300
max_p_extend_w                  =   1300
/
!max_error_dewpoint             =   20
!max_buddy_dewpoint             =   20
!qc_psfc                        =   .TRUE.
use_p_tolerance_one_lev         =   .TRUE.
max_p_tolerance_one_lev_qc      =   800

&record5
print_obs_files                 =   .TRUE.
print_found_obs                 =   .FALSE.
print_header                    =   .FALSE.
print_analysis                  =   .FALSE.
print_qc_vert                   =   .FALSE.
print_qc_dry                    =   .FALSE.
print_error_max                 =   .FALSE.
print_buddy                     =   .FALSE.
print_oa                        =   .FALSE.
/

&record7
use_first_guess                 =   .TRUE.
f4d                             =   .TRUE.
intf4d                          =   21600
lagtem                          =   .FALSE.
/

&record8
smooth_type                     =   1
```

```
 smooth_sfc_wind              =  0
 smooth_sfc_temp              =  0
 smooth_sfc_rh                =  0
 smooth_sfc_slp               =  0
 smooth_upper_wind            =  0
 smooth_upper_temp            =  0
 smooth_upper_rh              =  0
 /

 &record9
 oa_type                      =  'Cressman'
 radius_influence             =  5,4,3,2
 mqd_minimum_num_obs          =  30
 mqd_maximum_num_obs          =  1000
 oa_min_switch                =  .TRUE.
 oa_max_switch                =  .TRUE.
 /
 oa_3D_option                 =  1
 oa_3D_type                   =  'Cressman'
 scale_cressman_rh_decreases  =  .TRUE.
 radius_influence_sfc_mult    =  0.4
 oa_psfc                      =  .FALSE.
 max_p_tolerance_one_lev_oa   =  700


 &plot_sounding
 file_type                    =  'raw'
 read_metoa                   =  .TRUE.
 /
 file_type                    =  'used'
```

A.2 March 2010 Dust Event

namelist.input

```
 &time_control
 run_days                     =        0
 run_hours                    =        0
 run_minutes                  =        0
 run_seconds                  =        0
```

```
start_year                          =        2010
start_month                         =        3
start_day                           =        1
start_hour                          =        18
end_year                            =        2010
end_month                           =        4
end_day                             =        10
end_hour                            =        18
interval_seconds                    =        21600
input_from_file                     =        .true.
history_interval                    =        60
frames_per_outfile                  =        1000
restart                             =        .false.
restart_interval                    =        7200
io_form_history                     =        2
io_form_restart                     =        2
io_form_input                       =        2
io_form_boundary                    =        2
io_form_auxinput2                   =        2
auxinput4_inname                    =        wrflowinp_d<domain>
auxinput4_interval                  =        360
io_form_auxinput4                   =        2
auxinput11_interval                 =        1
auxinput11_end_h                    =        99999
force_use_old_data                  =        T
/

&domains
time_step                           =        10
time_step_fract_num                 =        0
time_step_fract_den                 =        1
max_dom                             =        1
e_we                                =        106
e_sn                                =        106
e_vert                              =        33
p_top_requested                     =        5000
num_metgrid_levels                  =        27
num_metgrid_soil_levels             =        4
dx                                  =        10000
dy                                  =        10000
grid_id                             =        1
```

```
parent_id                   =       1
i_parent_start              =       1
j_parent_start              =       1
parent_grid_ratio           =       1
parent_time_step_ratio      =       1
feedback                    =       1
smooth_option               =       0
sfcp_to_sfcp                =       .true.
/

&physics
mp_physics                  =       8
cu_physics                  =       6
ra_lw_physics               =       4
ra_sw_physics               =       4
bl_pbl_physics              =       7
sf_sfclay_physics           =       7
sf_surface_physics          =       7
radt                        =       30
bldt                        =       0
cudt                        =       5
icloud                      =       1
num_land_cat                =       40
num_soil_layers             =       2
sf_urban_physics            =       1
pxlsm_modis_veg             =       1
sst_update                  =       1
pxlsm_smois_init            =       1
/

&fdda
pxlsm_soil_nudge            =       1
grid_fdda                   =       1
gfdda_inname                =       wrffdda_d<domain>
gfdda_interval_m            =       360
gfdda_end_h                 =       99999
io_form_gfdda               =       2
fgdt                        =       0
if_no_pbl_nudging_uv        =       0
if_no_pbl_nudging_t         =       1
if_no_pbl_nudging_q         =       0
```

if_zfac_uv	=	0
k_zfac_uv	=	10
if_zfac_t	=	0
k_zfac_t	=	10
if_zfac_q	=	0
guv	=	0.0001
gt	=	0.0001
gq	=	0.00001
if_ramping	=	1
dtramp_min	=	60
grid_sfdda	=	1
sgfdda_inname	=	wrfsfdda_d<domain>
sgfdda_end_h	=	99999999
sgfdda_interval_m	=	360
sgfdda_interval	=	21600
guv_sfc	=	0
gt_sfc	=	0
gq_sfc	=	0
rinblw	=	250
obs_nudge_opt	=	0
max_obs	=	300000
fdda_start	=	0
fdda_end	=	99999
obs_nudge_wind	=	0
obs_coef_wind	=	0.0006
obs_nudge_temp	=	0
obs_coef_temp	=	0.0006
obs_nudge_mois	=	0
obs_coef_mois	=	0.0006
obs_rinxy	=	240
obs_rinsig	=	0.1
obs_twindo	=	0.666667
obs_npfi	=	10
obs_ionf	=	2
obs_idynin	=	0
obs_dtramp	=	40
obs_prt_freq	=	10
obs_prt_max	=	10
obs_ipf_errob	=	.true.

```
obs_ipf_nudob           =       .true.
obs_ipf_in4dob          =       .true.
/

&dynamics
hybrid_opt              =       2
w_damping               =       0
diff_opt                =       1
km_opt                  =       4
diff_6th_opt            =       0
diff_6th_factor         =       0.12
base_temp               =       290
damp_opt                =       3
zdamp                   =       5000
dampcoef                =       0.2
khdif                   =       0
kvdif                   =       0
non_hydrostatic         =       .true.
moist_adv_opt           =       1
scalar_adv_opt          =       1
gwd_opt                 =       1
epssm                   =       0.1
/

&bdy_control
spec_bdy_width          =       5
specified               =       .true.
/

&grib2
/

&namelist_quilt
nio_tasks_per_group     =       0
nio_groups              =       1
/
```

namelist.oa

```
 &record1
 start_year                      =       2010
 start_month                     =       3
 start_day                       =       1
 start_hour                      =       18
 end_year                        =       2010
 end_month                       =       4
 end_day                         =       10
 end_hour                        =       18
 interval                        =       21600
 /

 &record2
 grid_id                         =       1
 obs_filename                    =       'SURFACE_OBS'
 remove_data_above_qc_flag       =       32768
 remove_unverified_data          =       .TRUE.
 /
 obs_filename                    =       '.'
 trim_domain                     =       .TRUE.
 trim_value                      =       5

 &record3
 max_number_of_obs               =       400000
 fatal_if_exceed_max_obs         =       .TRUE.
 /

 &record4
 qc_test_error_max               =       .TRUE.
 qc_test_buddy                   =       .FALSE.
 qc_test_vert_consistency        =       .TRUE.
 qc_test_convective_adj          =       .TRUE.
 max_error_t                     =       10
 max_error_uv                    =       13
 max_error_z                     =       8
 max_error_rh                    =       50
 max_error_p                     =       600
 max_buddy_t                     =       8
 max_buddy_uv                    =       8
 max_buddy_z                     =       8
 max_buddy_rh                    =       40
```

```
max_buddy_p                =       800
buddy_weight               =       1
max_p_extend_t             =       1300
max_p_extend_w             =       1300
/
!max_error_dewpoint        =       20
!max_buddy_dewpoint        =       20
!qc_psfc                   =       .TRUE.
use_p_tolerance_one_lev    =       .TRUE.
max_p_tolerance_one_lev_qc =       800

&record5
print_obs_files            =       .TRUE.
print_found_obs            =       .FALSE.
print_header               =       .FALSE.
print_analysis             =       .FALSE.
print_qc_vert              =       .FALSE.
print_qc_dry               =       .FALSE.
print_error_max            =       .FALSE.
print_buddy                =       .FALSE.
print_oa                   =       .FALSE.
/

&record7
use_first_guess            =       .TRUE.
f4d                        =       .TRUE.
intf4d                     =       21600
lagtem                     =       .FALSE.
/

&record8
smooth_type                =       1
smooth_sfc_wind            =       0
smooth_sfc_temp            =       0
smooth_sfc_rh              =       0
smooth_sfc_slp             =       0
smooth_upper_wind          =       0
smooth_upper_temp          =       0
smooth_upper_rh            =       0
/

&record9
oa_type                    =       'Cressman'
radius_influence           =       5,4,3,2
```

```
mqd_minimum_num_obs      =      30
mqd_maximum_num_obs      =      1000
oa_min_switch            =      .TRUE.
oa_max_switch            =      .TRUE.
/
oa_3D_option             =      1
oa_3D_type               =      'Cressman'
scale_cressman_rh_decreases =   .TRUE.
radius_influence_sfc_mult =     0.4
oa_psfc                  =      .FALSE.
max_p_tolerance_one_lev_oa =    700


&plot_sounding
file_type                =      'raw'
read_metoa               =      .TRUE.
/
file_type                =      'used'
```